**ORIGINAL ARTICLE**

CrossMark

# Friction stir welding of dissimilar aluminum alloys and steels: a review

Long Wan[1] · Yongxian Huang[1]

## Abstract

The present paper is focused on friction stir welding (FSW) of dissimilar aluminum alloys and steels, an area that is getting great concern recently. The promise of FSW joints lies in low welding heat input and its ability to minimize the extent of the formation of intermetallic compound (IMC) in dissimilar metals. The present paper assessed the status of FSW process of dissimilar aluminum alloys and steels, and to identify the opportunities and challenges for the future. The essential reason for the formation of the dissimilar Al/steel FSW joints with high quality is explained by super diffusion behavior. This paper will provide basis to designers and engineers to consider FSW for a wider range of dissimilar aluminum alloys and steels.

**Keywords** Friction stir welding · Aluminum alloys · Steels · Intermetallic compound · Super diffusion behavior

## 1 Introduction

Energy and environmental issues in industries have strong influence on material selection and on the development of joining techniques [1–4]. The combination of light-weight materials in many structures allows a reduction of weight and fuel consumption. Figure 1 shows the applications of Al/steel hybrid structures in the automotive, ship-building, and aerospace industries. Dissimilar joining of steels to aluminum alloys attracts great interest both in science and industrial applications [5–11]. It allows the use of the aluminum alloys and steels in the same design [12]. The high strength, good creep resistance, and formability of steels may be combined with the low density, high thermal conductivity, and good corrosion resistance of aluminum alloys in one hybrid structure. Applications of dissimilar Al/steel joints are very common. The introduction of engineering material of aluminum alloys in a standard steel car body is an attractive compromise between cost and performance [13]. An example of the industrial use of dissimilar friction stir welding (FSW) came from the Honda Motor Co. which used FSW to realize lap joining of the Al and steel in engine cradles. Another example was joining aluminum alloy to stainless steel for application in the field of cryogenics, in which cryogenic liquid was stored in aluminum alloy chambers and transferred through stainless steel pipeline [14].

However, diverse lattice parameters, heat conductivity, and thermal expansion coefficients between steels and aluminum alloys make them difficult to join together, especially by conventional fusion welding. The major joining difficulties include four aspects. First, there is low solid solubility of Fe in Al, which is nearly zero under normal temperature. The solid solubility limit of Fe in Al is 0.01–0.022% at temperature ranging from 225 to 600 °C, as shown in Fig. 2. It will lead to welding defects like solidification and liquation cracks and porosity during welding process. Then, the interfacial zone of Al/steel joint is easy to generate brittle intermetallic compounds (IMCs) such as $FeAl_2$, $FeAl_3$, $Fe_2Al_5$, etc. which lead to the crack formation, resulting in the welding residual stress. For another aspect, the refractory $Al_2O_3$ oxide film is easy to form on the surface of aluminum alloy under the high temperature during the fusion welding process, which results in slag inclusion in the weld and then the performance degradation of the joints. At last, liquid aluminum alloy has poor wetting and spreading properties on uncoated steel sheets.

The current welding methods, such as low energy input fusion welding, brazing, and so on, can induce the formation of IMC layer with a certain thickness. The evolution of brittle IMCs, which are generated during the interfacial reaction between solid steel and liquid aluminum, can significantly influence the mechanical properties of Al/steel joints. Therefore, new methods are needed to realize the rapid development of the welding of dissimilar aluminum alloys and steels.

✉ Long Wan
wanlong178@163.com

[1]  State Key Laboratory of Advanced Welding and Joining, Harbin Institute of Technology, Harbin 150001, People's Republic of China

Fig. 1 The typical applications of Al/steel hybrid structures in industries. **a** Aerospace industry, **b** automotive industry, and **c** ship-building industry

In recent years, researchers had carried out a series of methods on the joining of dissimilar aluminum alloys and steels, involving arc welding brazing, laser welding, electron beam welding, diffusion welding, resistance spot welding, friction stir welding, etc. [9, 15, 16]. Recently, a mechanical joining method named self-piercing riveting technology was developed to realize the joining of aluminum alloy and steel [17–19], as shown in Fig. 3. This joining process does not involve the melting and solidification process of base material (BM), avoiding the formation of brittle IMCs. However, there exists some disadvantages such as no metallurgical bonding, low joint strength, poor air tightness, and especially the weak fatigue performance limiting the application. In order to realize metallurgical bonding and to control the formation of brittle IMCs, arc welding brazing was proposed. The different heating modes including arc, laser, and electron beam were used to make the aluminum alloys and filler metal melt [20–27]. However, the heterogeneity of the interfacial reaction was still not solved effectively, and a non-uniform IMC layer was formed through the thickness direction caused by the

uneven spatial energy distribution of the arc and the relatively low welding speed. At the same time, the auxiliary methods including hot dip aluminizing process, surfacing, adding intermediate layer, or adding trace elements had been used to restrain the formation of the IMCs [26, 28]. Although there were many methods focusing on joining aluminum alloys to steels, controlling the heat input to realize the optimization of interfacial zone was the research focus [29, 30]. To further improve the reliability of Al/steel joints, it is prone to apply the solid-state welding methods.

For solid-state joining, the main challenges are large differences in the thermal and mechanical characteristics of dissimilar aluminum alloys and steels, as well as the tendency for the formation of brittle IMCs. Friction stir welding (FSW) was invented at The Welding Institute (TWI) of UK in 1991 as a solid-state joining technique, and has now become an important process in the joining of aluminum alloys and other materials which are relatively soft compared with the tool used for stirring the metal [31–38]. A rotating tool with a specially designed pin and shoulder is inserted into the abutting edges
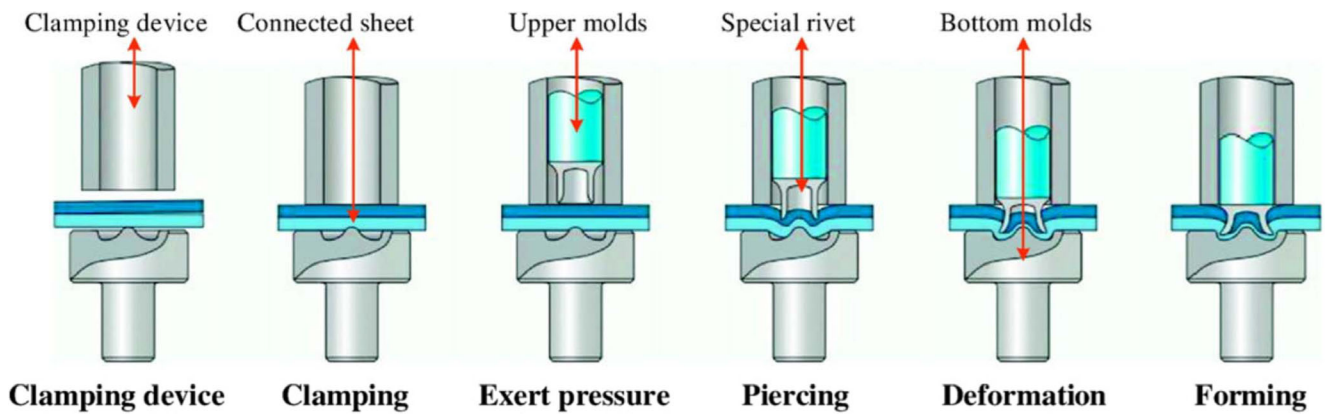
Fig. 2 The Al-Fe phase diagram
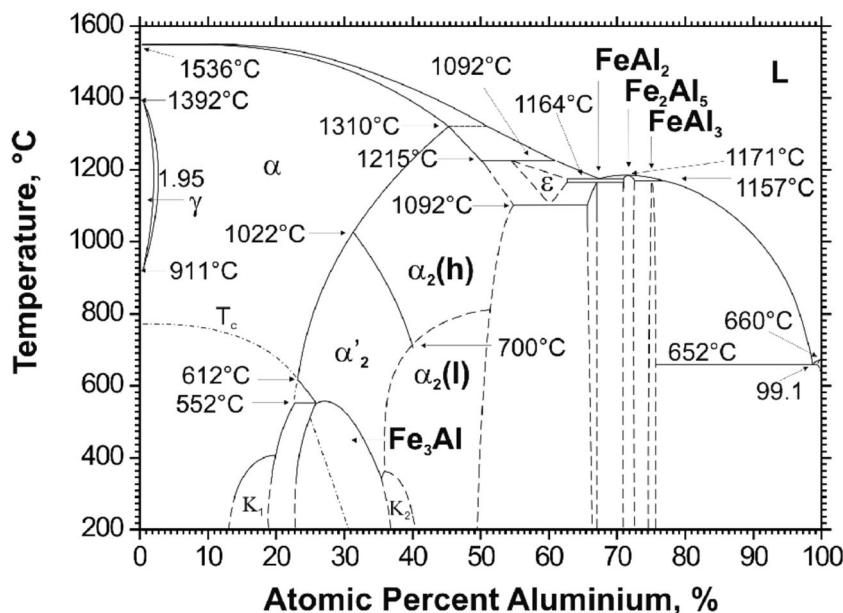
**Fig. 3** Schematic diagram of the forming process of a self-piercing rivet joint [19]

and traverses along the joint line [32–34], as shown in Fig. 4. The tool shoulder and probe have different shapes according to the variations of the base materials. The shoulder makes firm contact with the top surface. Heat generated by friction at the shoulder and to a lesser extent at the pin surface softens the material being welded. The common problems of fusion welding such as the solidification and liquation cracking, porosity, and the loss of volatile alloying elements are avoided due to the lack of melting in FSW [35–38]. These advantages are the main reasons for its widespread commercial success for the welding of aluminum and other soft alloys. However, the FSW tool is subjected to severe stress and high temperatures particularly for the welding of hard alloys. The cost-effective FSW tools are needed for welding some of these materials with high melting temperatures such as steels and titanium alloys [38–40].

The paper critically examines the current status, problems, and opportunities for the FSW techniques of dissimilar aluminum alloys and steels. The joint configurations range from butt to lap joints. There is a wealth of data on process development of welding variable windows for sound FSW welds, microstructural characterizations, material flow, failure modes, the role of the IMCs, and atom diffusion.

## 2 The tool material, design, and joint configurations

The FSW tool wear is a critical problem when dissimilar material welding involves at least one high-temperature material. Although it has been shown that sound welds may be achieved without plunging the welding tool into hard material
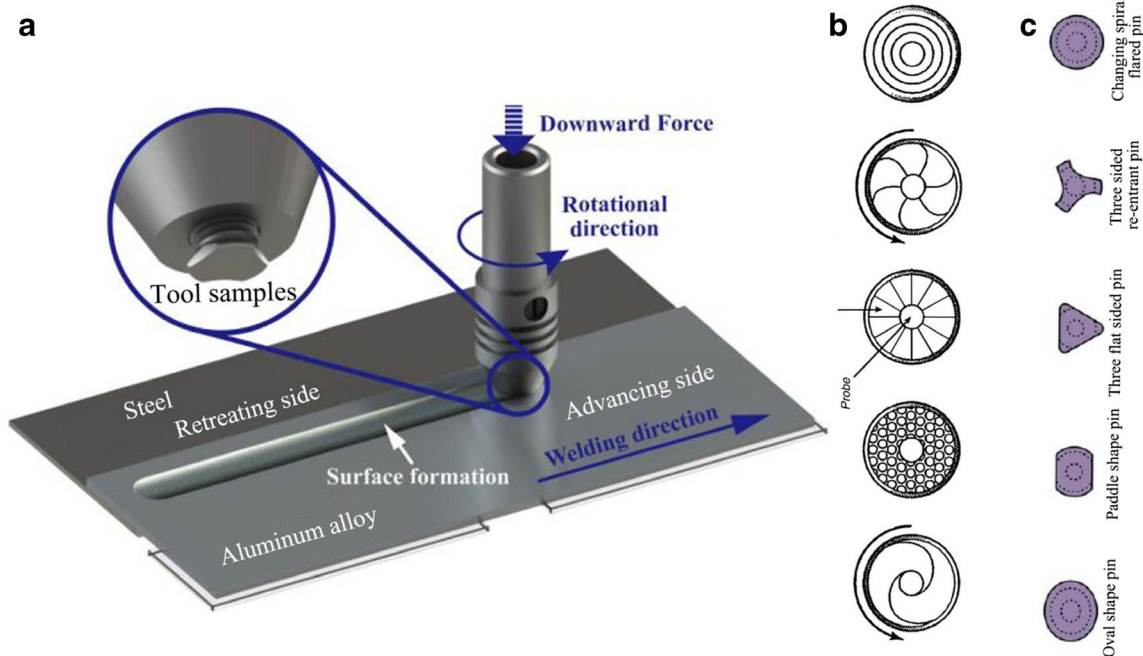


**Fig. 4** Schematic diagram of FSW process. **a** Basic FSW process, **b** different tool shoulders, and **c** different pin shapes

side, the FSW tool may be significantly worn during the joining of dissimilar aluminum alloys and steels due to the high yield strength and melting point of steels. The tool wear significantly affects the mechanical performance and quality of the joint. For solving the tool wear problem and improving tool service life, there have been several studies on the choice of tool material, tool design, and the joint configurations.

## 2.1 The choice of tool material

Weld quality, tool wear, and cost are three important considerations in the selection of tool material. The selection mainly depends on the workpiece material to be welded, cost effectiveness of tool material, and associated machining cost to desired shape. How easily the workpieces can be welded without defects and detrimental IMC with acceptable tool life specifies the requirement on tool material. The tool wear needs to be considered when welding is performed between dissimilar aluminum alloy to steels because of the high hardness and about 1500 °C melt temperature of the steel. The high process forces in combination with the arising temperatures demand the usage of high-temperature-resistant tool materials, which exhibits little wear. Suitable tool materials are beneficial to the weld quality and plastic deformation by increasing the friction coefficient and improving the heat input. The tool materials such as tool steel, mold steel, nickel-based super alloys, tungsten carbide, and tungsten-rhenium were commonly used for FSW of dissimilar aluminum alloys and steels [4, 7, 8, 13, 14, 41–59]. Table 1 shows the summary of the most frequently used tool materials for Al/steel dissimilar FSW process. During FSW process, material mixing between dissimilar aluminum alloy and steel via shoulder friction, pin stirring, or scribing is required for the improvement of mechanical properties by means of preventing IMC thickening and forming either a metallurgical bonding or a mechanical interlocking. Depending on types of steels and aluminum alloys to be welded, different kinds of tool steels and alloy steels had been used in both lap and butt configurations. Chen et al. [60] used friction stir lap welded (FSLW) 6060 aluminum alloy to mild steel using tool steel as tool material and reported no significant wear of tool pin even when the pin was plunged into the mild steel by 0.1 mm. Haghshenas et al. [61] welded AA5754 aluminum alloy with high strength steels DP600 and 22MnB5 in lap joint configuration using tool steel as tool material without its excessive wear by placing the softer aluminum alloy on top of the steel plates and avoiding direct contact of the tool with the steel plates. Chen and Kovacevic [8] joined Al6061 to AISI 1018 steel sheet with the thickness of 6 mm and observed that the tool was significantly worn and broken during the welding process which affected the final formation of the weld. The on-line acoustic emission monitoring system was applied to detect the tool wear conditions. Figure 5 showed the related wavelet transform results as an aerial view and contour map. The difference in the band energy profile and contour map before and after the tool breakage was recognized and the position pointed out by the arrows indicated the tool breakage.

Tungsten-based tools such as tungsten rhenium and tungsten carbide are necessary if the tool will be plunged in the hard material and subjected to severe frictional conditions. Liyanage et al. [62] used W-25Re tool to make dissimilar friction stir spot welds between aluminum alloy and steel, and between magnesium alloy and steel with report of some tool wear. Bozzi et al. [63] applied W-25Re to friction stir spot welded AA6016 aluminum alloy and IF steel. Liu et al. [52] butt welded AA6061 aluminum alloy and high-strength TRIP 780/800 steel using WC-10% Co by slightly offsetting pin to Al side. High-temperature-resistant coatings can further prevent tool wear. Habibnia et al. [50] friction stir welded 5050 aluminum alloy and 304 stainless steel plates using a tungsten carbide tool and indicated that no tool wearing occurred during the welding process. Coelho et al. [4] butt welded AA6181-T4 aluminum alloy and HSS high-strength steel with W-25Re tool and minimum tool wear occurred. Pourali et al. [64] friction stir lap welded 1100 aluminum alloy and St37 steel with the tool made of tungsten carbide with a non-threaded conical pin. The tool contacted with the steel and the tool wear took place at higher rotational speeds because of an increase in strain rate.

Since part of the FSW tool would be immersed in the steel side and subjected to severe frictional conditions, refractory materials such as $Si_3N_4$ and polycrystalline cubic boron nitride (PCBN) were required for the tools [65]. The PCBN was a preferred tool material due to its high strength and hardness at elevated temperatures along with high-temperature stability and could resist wear when it was plunged into the lower steel deeply. The PCBN tool could relieve tool wear to some extent, but could not also realize the long distance welding [66]. At the same time, the cost for making PCBN tool is very high due to critical manufacturing processes which require high temperatures and pressures. Sawada and Nakamura [67] successfully lap welded 3-mm-thick stainless steel 304 to a same thickness ductile cast iron FCD450 using a PCBN tool by preheating the workpieces. Choi et al. [68] butt welded a 4-mm-thick low-carbon steel SPHC to a high-carbon steel SK85 with PCBN tool and reported superior tensile property comparable to SPHC. The combined welding tool consisted of die steel shoulder and tungsten carbide pin was also developed. Yasui et al. [55] chose the die steel and WC-Co alloy steel as the shoulder and stir pin materials respectively to increase the friction heat and improve the tool wear resistance.

## 2.2 The tool shape and design

Tool design is one of the most influential aspects of FSW process development. Tool geometry affects the frictional heat generation and plastic material flow and further influences

**Table 1** Summary of the most frequently used tool materials for Al/steel dissimilar FSW
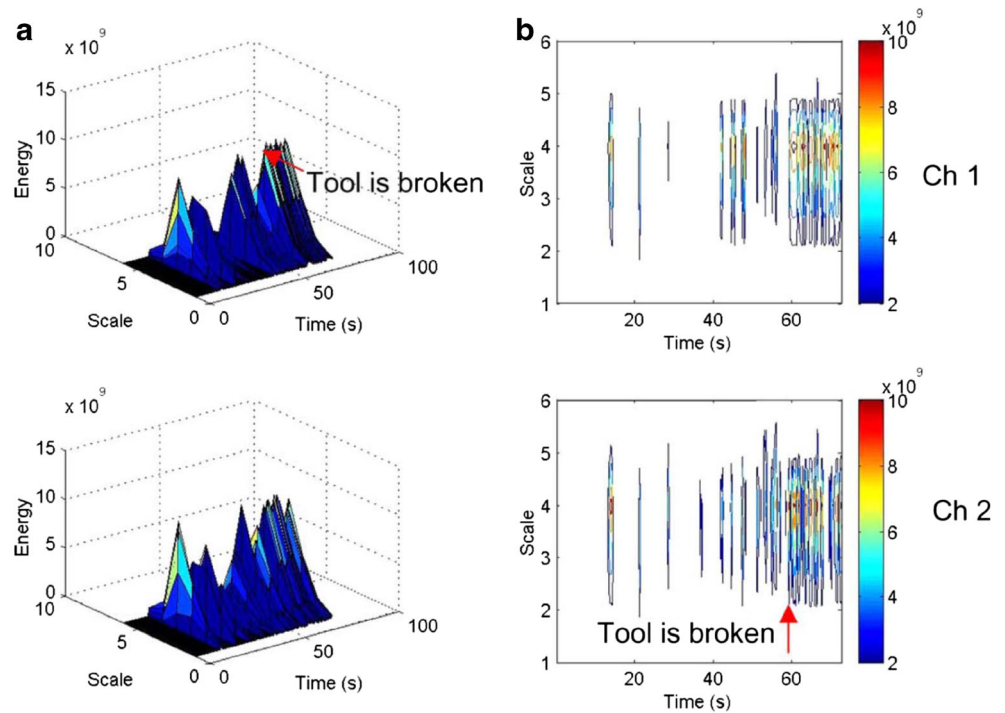
| Base materials | Joint configuration | Tool materials | References |
|---|---|---|---|
| 6061 Al, AISI 1018 steel | Butt joint | H13 tool steel | [8, 41] |
| 5083 Al, 316L stainless steel | Butt joint | H13 tool steel | [42] |
| 6061 Al, SS400 mild steel | Butt joint | AISI 4140 tool steel | [43] |
| 6082 Al, mild steel | Butt joint | AISI 4140 tool steel | [13] |
| 5083 Al, SS400 mild steel | Butt joint | Heat-treated tool steel | [7] |
| 5083 Al, SS400 mild steel | Lap joint | JIS-SKH57 tool steel | [44] |
| Pure Al, mild steel | Lap joint | SKD61 tool steel | [45] |
| 5083 Al, ST12 mild steel | Lap joint | H13 tool steel | [30] |
| 6061 Al, SUS304 steel | Lap joint | SKD tool steel | [46] |
| Pure Al, zinc-coated mild steel | Lap joint | SKD61 tool steel | [47] |
| 6061Al, DC04steel | Butt joint | Nickel-base alloy | [48] |
| LF6 Al, ST12 mild steel | Butt joint | Super alloy | [49] |
| 5050 Al, 304 stainless steel | Butt joint | Tungsten carbide | [50] |
| 6061 Al, 304 stainless steel | Butt joint | Tungsten carbide | [51] |
| 6061 Al, TRIP steel | Butt joint | Tungsten carbide | [52] |
| ADC12 Al, SS400 mild steel | Butt joint | Tungsten carbide | [53] |
| 3003 Al, SUS304 steel | Lap joint | Tungsten carbide | [2] |
| 6181 Al, DP600 and HC260LA high strength steel | Butt joint | Tungsten–Rhenium WRe25 | [4] |
| 5754 Al, DP600 dual phase steel | Lap joint | WC cermet | [54] |
| 6063 Al, S45C steel | Butt joint | SKD61 tool steel shoulder, tungsten carbide pin | [55] |
| Pure Al, interstitial free steel | Butt joint | High speed steel shoulder, tungsten carbide pin | [56] |
| 6061 Al, Q235 steel | Butt joint | Tungsten and molybdenum alloy | [57] |
| Pure Al, 304 stainless steel | Butt joint | Die steel shoulder, tungsten carbide pin | [14] |
| 6082 Al, S355J2 + N steel | Lap joint | M42 mold steel shoulder, tungsten carbide pin | [58] |
| Pure Al, stainless steel | Lap joint | H13 tool steel shoulder, YG8 cemented carbide pin | [59] |

microstructure and mechanical properties. Compared to FSW of similar materials, the tool geometry plays a more critical role in FSW dissimilar aluminum alloys and steels. When designing a tool, attention needs to be paid to defect formation and IMC formation. Due to the asymmetrical temperature generated during FSW and intrinsic physical property differences, it is expected that the material flow in the weld zone would be more inhomogeneous compared to FSW joint of similar materials and researchers have more challenges to achieve defect-free welds. Both defects and IMC formation are directly linked to material mixing between dissimilar aluminum alloys and steels via pin stirring and scribing is required for mechanical performance by disrupting the tenacious oxide layer present on the surfaces, preventing IMC thickening and forming either a metallurgical bonding or a mechanical interlocking. The tool design influences the degree of the two materials mixing during welding. Important factors include shoulder diameter, shoulder surface feature, pin shape, size, and additional surface features. The FSW tool commonly consists of the convex scroll, concave

or flat shoulders, and conical or cylindrical pin. Figure 6 showed different kinds of FSW tool shapes and designs used for realizing the joining of aluminum alloy and steel. Shamsujjoha et al. [69] FSLW welded aluminum alloy to steel using refractory metal pin tools with featureless tapered geometries and investigated the combined effects of plunge depth and bonding area on joint properties. Mahto et al. [70] used the FSW tool with a cylindrical pin to realize lap joining of 6061-T6 aluminum alloy and AISI304 stainless steel. Pourali et al. [64] FSLW welded Al 1100 and St37 steel with the tool made of tungsten carbide with a non-threaded conical pin to avoid severe wear and tool fracture conditions. A FSW tool with a screw thread probe made of SKD61 tool steel was used to realize the Al/steel joining [71].

In order to avoid severe tool wear and ensure the sufficient plastic flow of the material, researchers had developed special stir pins with scraping or cutting specialty on the basis of commonly used tools [59, 72]. Pins with cutting feature had been developed for lap welding of low- and high-melting-

temperature material by scribing the high-melting-temperature material to create either metallurgical bonding or mechanical interlocking. Xiong et al. [59] reported sound lap welds between AA1060 aluminum alloy and stainless steel SUS321 using a tungsten carbide pin with cutting edges which exhibited good wear resistance. Same pin design was applied to dissimilar lap welding of AA1060 to titanium alloy Ti-6Al-4V [73] and AZ31 magnesium alloy to stainless steel SUS321 [74]. The

short WC insert was plunged into the lower steel and acted as a cutter to deform the steel and mix it with upper Mg. Sorger et al. [75] developed an innovative overlap joint concept to evaluate the quality improvement of joints between AA5754-H22 aluminum alloy and DX54 steel. The wave-shaped interface was produced on the steel being directly processed by the tip of the probe, generating localized heat, extensive chemically active surfaces, and additional mechanical interlocking. FSW tool
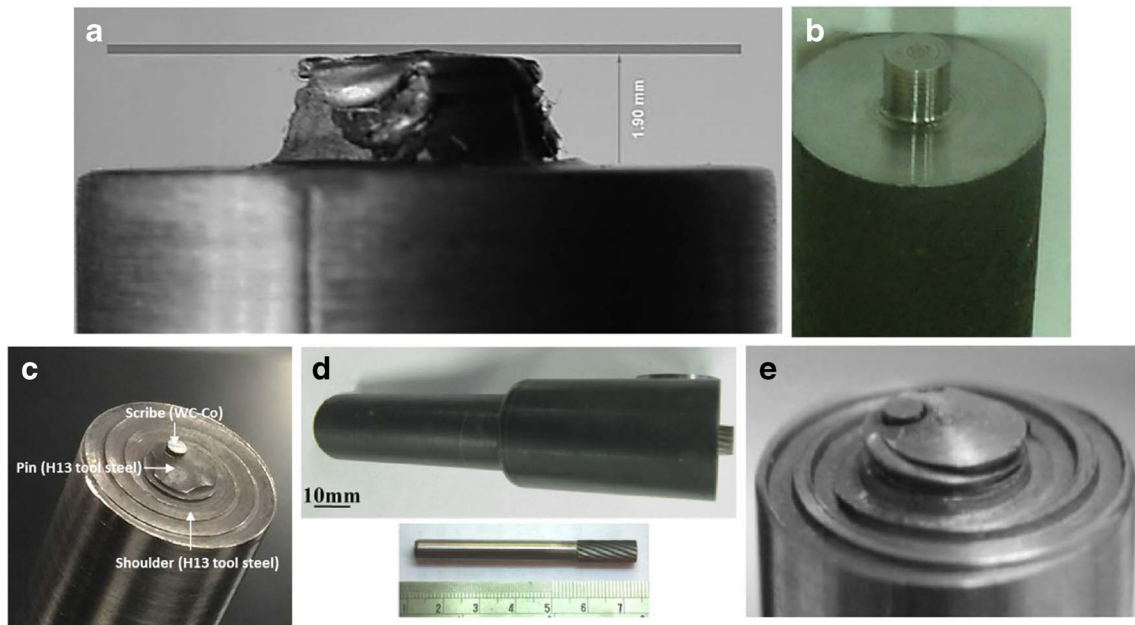


Fig. 6 Different kinds of FSW tool shapes and designs. **a** Conical stir pin, **b** cylindrical stir pin, **c** tool with scribe made of tungsten carbide-cobalt cermet, **d** cutting pin with rotary burrs, and **e** scrolled tool with scribe affixed to pin tip

without stir pin was also developed to realize the lap and spot welding of aluminum alloy to steel by friction between the shoulder and the upper material. However, the thickness of the material being able to be joined was restricted and was generally not more than 2 mm. Meanwhile, the plunge depth of shoulder was large, resulting in the severe welding flash and thinning significantly [76–78]. Zhang et al. [79] proposed friction stir brazing (FSB) technique for joining Al to steel to avoid the wear of pin by steel, in which a tool without pin was used. Chen et al. [80] investigated the FSLW feasibility of AC4C cast aluminum alloy and low-carbon zinc-coated steel. With appropriate welding parameters, full-strength joints could be obtained and joints fractured at the zinc-coated steel base material side.

## 2.3 Joint configurations

In FSW of aluminum alloy and steel which have very different thermo-physical properties, there are two kinds of joint configurations including butt and lap joints. Placing of dissimilar workpieces on advancing or retreating side and plunging rotating tool to a specific location relative to the joint interface in butt welding alters the weldability and impacts tool life. In butt joint configuration, the higher melting temperature workpiece was often placed on the advancing side and the welding tool was offset from the butt interface toward the lower melting temperature material to prevent tool wear and overheating of the lower melting temperature materials. For aluminum alloy and steel combination, the welding tool could not be plunged symmetrically into the joint line. It would result in excessive heating of steel which would cause melting of aluminum alloy BM. This phenomenon would result in a defective weld. Hence, for joining aluminum alloys and steels, the offset method was used during FSW, as shown in Fig. 7. In offset method, the rotation center of the tool was biased toward the aluminum alloy side, and in some cases to the extent that it almost plunged inside the aluminum alloy [10, 81]. When tool plunges completely inside aluminum alloys, such welds can be made using the tool used for making joining low-melting-point materials. Although the FSW tool should be shifted toward aluminum alloy in consideration of avoiding overheating of aluminum alloy, a part of the pin still need to remain in the steel side to actually stir both materials together. When the tool is making contact with the high-melting-temperature material, it becomes important to use ceramic-based tools or tools made of refractory metals. The work done by Watanabe et al. [7] showed the effect of tool pin offset on the joint integrity. The tool offset varied from the cylindrical surface of the tool pin being 0.2 mm away from the faying surface toward aluminum alloy to 2 mm inside steel workpiece. Among all, the weld with 0.2 mm pin offset toward steel exhibited maximum tensile strength. The joint efficiency of the weld corresponding to 0.2 mm offset toward steel side was approximately 85% of the aluminum alloy BM.

To avoid the melting of soft material during process, the pin must be plunged into this soft metal with the lower melting temperature and place as the retreating side in the joint design. The mechanism of joint formation between alloy aluminum and steel was proposed by Yazdipour and Heidarzadeh [82]. It was schematically shown in Fig. 8. The activated area belonged to the region that pin had just traveled and activated by rubbing motion of the rotating pin, as shown by bold line. When the pin rotation direction was clockwise, the steel was placed on the retreating side. The plastic deformed aluminum alloy made contact with the oxide film on the faying surface of steel and the whirling aluminum alloy was pressed into the unactivated area. Moreover, the tool tangential velocity on the retreating side could try to peel off already deposited layer on the retreating side. Hence, the formation of sound weld was very difficult. When the pin rotated counterclockwise, the steel was on the advancing side. The tool made contact with the steel and disrupted the continuous oxide film thereby exposing an activated layer of steel to aluminum alloy. The rotating aluminum alloy in its plastic deformation flow was pressed into the activated area just behind the traveled pin, which caused formation of good joint between both materials.

Placing of dissimilar workpieces in upper or lower sheet and plunging rotating tool to a specific location relative to the joint interface in lap welding alters the welding quality and influences tool life. Normally, the steel plate was usually placed under the aluminum alloy plate in FSLW of aluminum alloy and steel [30], as shown in Fig. 9a. However, a method that combined the effects of both fusion and solid-state welding was put forward by placing the steel plate upon the aluminum alloy plate [83], as shown in Fig. 9b. Frictional heat was generated due to the intimate contact between the pressed rotating tool and the top steel sheet. In addition, plastic deformation occurred below the rotating tool, also contributing to the temperature increase. The generated heat was transmitted to the bottom sheet through the top sheet and the low-melting-point bottom aluminum alloy sheet partially melts, forming a localized pool of liquid metal in contact with the upper sheet. In contrast to conventional fusion welding processes, the melting temperature of the low-melting-point material was only exceeded slightly and very locally, resulting in a semi-solid welding process. The surface frictional heat was taken as the heat source and the heat input at the interface was guaranteed by heat transfer. However, the thickness of the steel plate was limited and generally did not exceed 1 mm.

## 2.4 Auxiliary modes

To felicitously combine superiorities of both aluminum alloys and steels, a proper joining method is essential. The hard and brittle IMCs are difficult to avoid, which are detrimental to mechanical properties of the joints. To strengthen Al/steel dissimilar FSW joints, a novel concept with assistance of mechanical interlocking via prefabricated geometrical
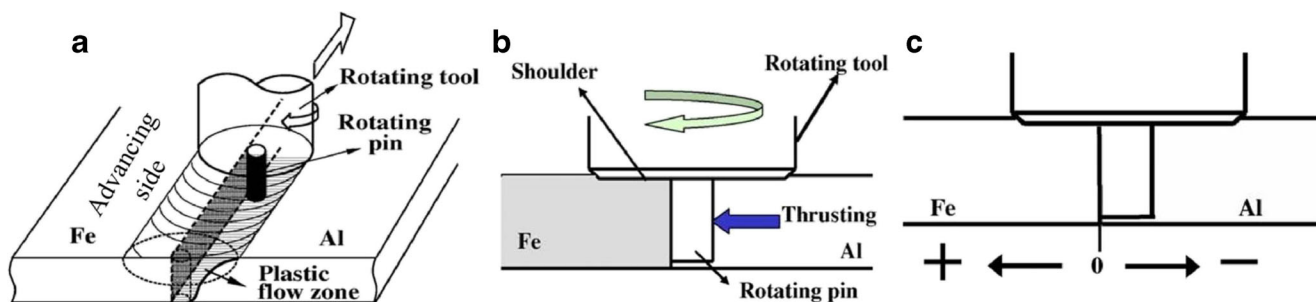
**Fig. 7** Schematic illustration of FSW butt joining of 5083 aluminum alloy and SS400 steel [7]. **a** The rotating pin position, **b** schematic view of the cross-section perpendicular to weld line, and **c** schematic illustration to explain the relationship between the pin position and the coordinate

configurations was developed. Evans et al. [84] joined aluminum alloy to steel with prefabricated concave and O-ring dovetail grooves. Plasticized aluminum was extruded into grooves and then mechanical interlocking was created. However, metallurgical bonding was absent, while grooves on steel also weakened the matrix. Huang et al. [85] put forward a new self-riveting FSLW technique. The plasticized aluminum alloy was forced into the prefabricated holes, producing self-riveting structure with metallurgical bonding at the Al/steel interface. Recently, fusion welding-assisted FSW methods with additional heat source were put forward to enhance the plastic flow of the deformed material and reduce the tool wear [57, 86, 87]. Laser-assisted FSW may be a potential solution to the above problems [57]. In laser-assisted FSW, the strength and hardness of steel were reduced obviously by placing a focused laser beam with high intensity in front of the rotating tool in the steel side to preheat the steel, which realized simultaneous softening of steel and aluminum alloy, improved the flow ability and mixture of the materials, reduced the wear of the stir pin, and limited the formation of the IMCs. In laser-assisted FSW of aluminum alloy and steel, suitable preheating temperature of the steel was very important either for reducing the too wear or for obtaining a sound joint. Electrically assisted FSW method was developed for joining 6061 aluminum alloy to TRIP780 steel by Liu et al. [88]. The axial welding force was effectively reduced with application of current especially when rotation speed was

lower and tool offset into aluminum was smaller. Enhanced formation of thin IMC layer and micro-interlock features at the interface were believed to be beneficial for joint quality. Table 2 shows the Al/steel FSW methods assisted with different auxiliary modes.

# 3 Process window and mechanical properties

## 3.1 Process window

Compared with similar materials FSW, the FSW of dissimilar aluminum alloys and steels has more welding parameters needing to adjust, as shown in Fig. 10. The main influence parameters include pin offset, plunge depth, welding speed, rotation speed, relative position, surface state, and so on. The welding parameters determine joint properties by controlling the distribution of welding energy as heat input or mechanical work. Tanaka et al. [6] reported the relationship between joint strength and heat input which was obtained using approximate expression based on equation of moving line source. At low welding speeds, mechanical work was the dominant factor. The optimum tensile strength was achieved at low welding speeds and high rotation speeds, where both factors of heat input and mechanical work were in equilibrium.

In dissimilar materials FSW butt joint, there are four major controllable factors, which are tool offset, tool rotation speed,
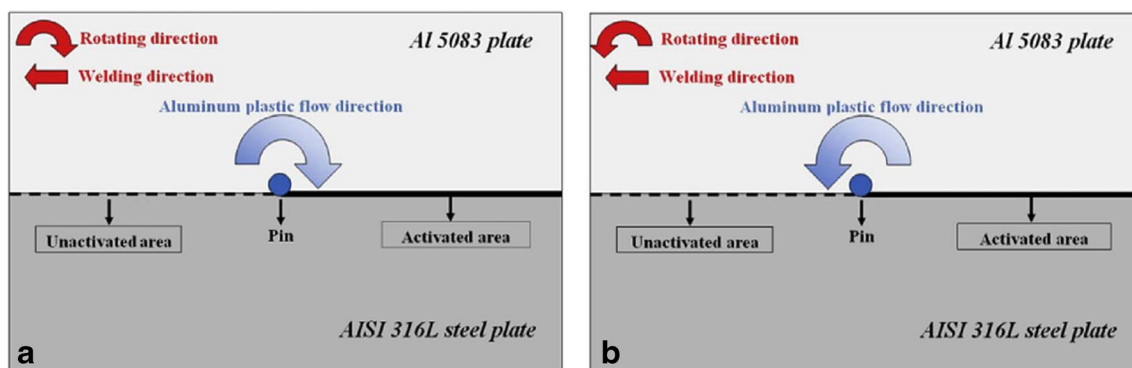


**Fig. 8** Schematic illustration explaining the reason why the counterclockwise rotation of a pin cannot weld aluminum to steel: **a** clockwise rotation of a pin and **b** counterclockwise rotation of a pin [82]
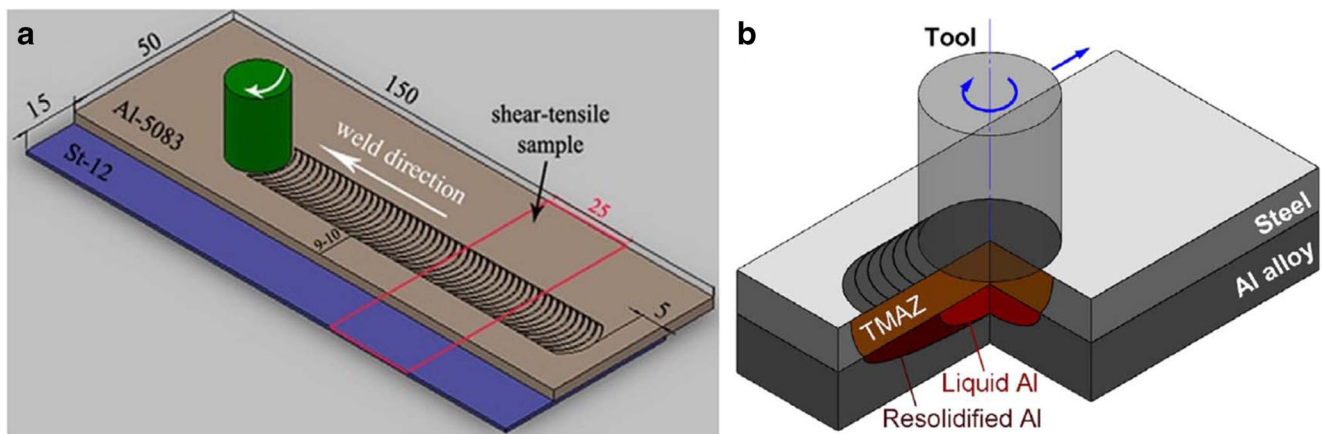
**Fig. 9** Schematic of the friction stir lap welding of aluminum alloy and steel. **a** Aluminum-to steel joint [30] and **b** steel-to-aluminum joint [83]

welding speed, tool tilt angle with respect to the workpiece surface, and pin tool diameter. Chen [43] investigated the influence of process parameters on FSW butt joints of Al6061-T651 aluminum alloy and SS400 steel, and indicated that rotation and welding speed were relatively more significant FSW process parameters compared to the tool tilt angle or pin diameter. The lower rotation speed and welding speed can result in higher impact values of joint strength. The effects of tool welding speed on the formation of IMCs, tunnel formation, and tensile strength of joints were investigated by Dehghani et al. [89]. At low welding speeds, due to the formation of thick IMCs in WNZ, the tensile strength of joints was very poor and the tunnel defect was formed. As the welding speed increased, the IMCs decreased and the joint exhibited higher tensile strength. The similar result was also reported by Derazkola et al. [90]. Another important factor for dissimilar FSW is the pin length or plunge depth. It is possible to achieve high-quality joints between Al and steel using FSW by carefully controlling the pin depth to avoid the formation of an Al-rich IMC layered structure. For butt welding, the pin length is generally very close to the total thickness of workpieces. In terms of lap welding, a pin length close to or slightly longer than the thickness of upper sheet workpiece was recommended for disrupting the surface oxide, creating intimate contact between fresh metal surfaces, and limiting IMC formation, in turn, obtaining a sound weld with good mechanical performance. Habibnia et al. [50] studied the effect of plunge depth of tool penetration on the joint quality. The tool penetration depths were chosen in three levels. For zero penetration, a tunnel was created in the welding zone. On the contrary, for 0.4 mm penetration, the stirred materials were splashed from the WNZ and flashes were created in the welding zone. The best result was obtained per 0.2 mm tool penetration. In this case, no defect was observed on the WNZ and surface of welded specimen. Elrefaey et al. [45] worked on the FSW of 1100 H24 aluminum alloy and low carbon steel with lap joint configuration. The joint strength depended strongly on the depth of the pin tip relative to the steel surface.
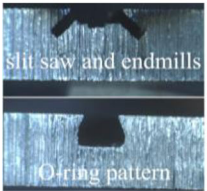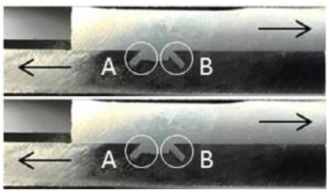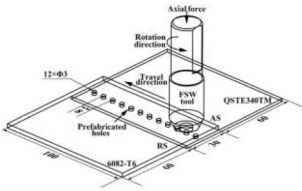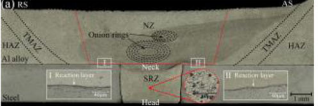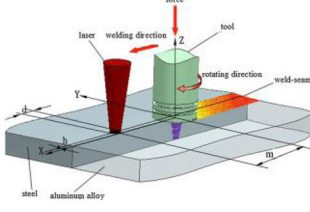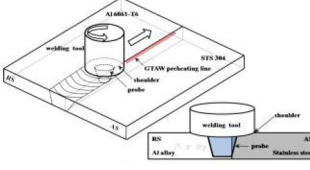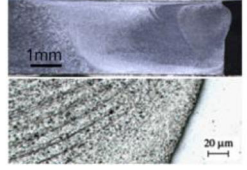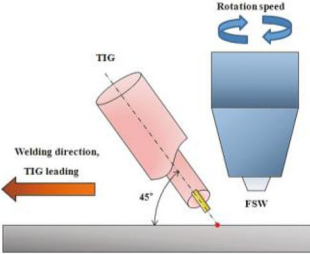
When the pin depth did not reach the steel surface, the joint failed under low applied loads. Meanwhile, slight penetration of the pin tip into the steel surface significantly increased the joint strength. It can be concluded that it is required to set an optimum tool plunge depth, enabling to minimize the pin penetration into the steel plate and, simultaneously, to promote the bonding between the two plates. Chen et al. [91] suggested that the Zn coating on steel could improve the weldability of Al and steel through promoting the formation of Al-Zn low-melting-point eutectic structure. They also reported in another study [92] on FSLW joint that the thickness of IMC layer increased from 7.7 to 58.1 μm with decreasing welding speed, which significantly affected the strength of the joint. The composition was identified to be mainly $Fe_2Al_5$ and $Fe_4Al_{13}$.

Generally, welding parameters such as tool rotation speed and welding speed are coupled to influence the frictional heat generation, volume of material movement, and disposition for a unit distance (ratio of tool rotation speed to welding speed). Normally, increasing the rotation speed or decreasing the welding speed within the appropriate range is conducive to plastic flow of weld metal and can get joints with good quality. However, when the heat input is too large to approach the melting point of the BM, it cannot form a good joint due to over softening. In addition, the increase of heat input will lead to the increase of the thickness of the Al-Fe IMC layer, and obviously reduce the mechanical properties of the joint. When the heat input is small, the high-melting-point material around the stir pin cannot be fully softened, resulting in the 'kiss' defect. Table 3 showed the main welding parameters of Al/steel FSW joints. In the Al/steel FSW butt welding, the increase of the thickness of base materials will narrow the selection of the welding parameters. Compared with butt joint, the range of welding parameters of lap joint is relatively wider.

## 3.2 Microhardness profiles

For Al/steel FSW joints at different welding speeds, the maximum microhardness values were all achieved at the joint

**Table 2** The Al/steel friction stir welding methods with different auxiliary modes

| Auxiliary modes | Schematic illustrations | Cross-section of the joint |
| --- | --- | --- |
| Friction stir extrusion [84] |  |  |
| Self-riveting FSLW [85] |  |  |
| Laser-assisted FSW [57] |  |  |
| Gas tungsten arc welding assisted FSW [86] |  |  |
| Tungsten inert gas welding assisted FSW [87] |  |  |

interface, as shown in Fig. 11. This was attributed to the fine grain structure of steel at this region and the impact strengthening effect of discontinuous IMC layers formed at the interface [42]. The microhardness of the WNZ presented an inhomogeneous distribution and exhibited variable values, which depended on the measured point of the hardness indenter because of the existence of the fine or coarse dispersed steel particles in the WNZ. The microhardness obtained was lower than the hardness of individual intermetallics. One of the reasons was that the literature values were from bulk IMCs. Under the real condition, due to the thin width of the reaction layer during microhardness determination close to the interface, the impression covered some region belonging to the matrix. This soft matrix effect lowered the microhardness value near the interface with respect to the individual hardness of different intermetallics. In addition, the microhardness in the lower mild steel plate was generally higher than that of the base metal, and the highest hardness value was found located in the center part of the welds. The center part of the mild steel plate plastically deformed during the flattening of the protuberance on the steel plate. Therefore, the higher hardness value was found almost in the center area of the steel plate and the hardness increase was mainly caused by strain hardening due to plastic deformation.

**Fig. 10** The major influence parameters of Al/steel FSW joints
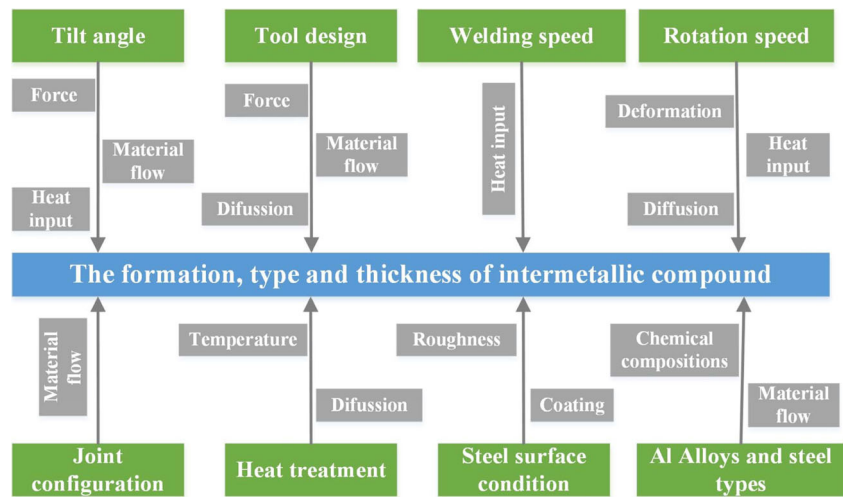


## 3.3 Failure modes

### 3.3.1 Butt joint

The fracture location in the dissimilar friction stir weld depends on the welding parameters [91]. Therefore, depending on the physical properties and weld microstructure of as-received material, the fracture path will either be through an interface, through another transition region, or through the base metal. Ghosh et al. [51] friction stir welded stainless steel to aluminum alloy and observed that fracture was initiated at the open end of the Al/steel joint, i.e., from the edge of the parallel length, as shown in Fig. 12, and propagated through the Al alloy/IMC interface. Ghosh et al. [14] studied the structural characterization of reaction zone for Al/steel FSW joint and found the ductile failure mode during the tensile test. The fracture took place primarily through the stirring zone of Al

substrate and the weakest region of this dissimilar assembly lay within the reaction zone. The reaction zone resembled composite microstructure as the intermetallics were dispersed within the Al BM. The inherent brittleness of the intermetallics lowered the bond strength. The IMC also restricted the material flow during tensile testing by their pinning action.

The pin offsets have great influences on the cross-sectional structures and fracture path of the joints [7]. Figure 13 showed the influences of a pin offset on the microstructure and fracture path of the joints. When the offset was zero or negative, removal of oxide film from the Fe faying surface was probably insufficient. Fracture of the joint occurred along the interface. When the pin offset became positive, the tensile strength increased and reached the maximum value at the offset of 0.2 mm. The fracture path of the joint shifted from the interface to Al matrix. When the offsets were 0.6 and 1 mm, steel fragments scattered in the Al matrix became larger in size and

**Table 3** Parts of the welding parameters for Al/steel FSW joints

| Base materials | Joint configuration | Thickness (mm) | Rotation speed (rpm) | Welding speed (mm/min) | Offset distance (mm) |
|---|---|---|---|---|---|
| 6061 Al, TRIP steel [52] | Butt join | Al 1.5, steel 1.4 | 1200–1800 | 30–120 | Into Al 0.325–0.925 |
| 6013 Al, X5CrNi18-10 [9] | Butt join | 4 | 800 | 80 | Into Al |
| Pure Al, 304 stainless steel [14] | Butt join | 2.5 | 1000 | 50 | Into Al |
| 6056 Al, 304 stainless steel [10] | Butt join | 3.0 | 800 | 80 | Into Al |
| 6061 Al, AISI 1018 steel [41] | Butt join | 6.0 | 914 | 140 | Into steel 0–5.5 |
| 6061 Al, SS400 mild steel [43] | Butt join | 6.0 | 550, 800 | 540, 720, 900 | Into steel 0.1–0.2 |
| 5083 Al, SS400 mild steel [7] | Butt join | 2.0 | 100–1250 | 25 | Into steel -0.2-2 |
| 5050 Al, 304 stainless steel [50] | Butt join | 3.0 | 500–710 | 40–80 | Into steel 1.5–3 |
| 6063 Al, S45C carbon steel [55] | Butt join | 5.0 | 1000–5000 | 200–1000 | Into steel 0.05 |
| ADC12 Al, SS400 mild steel [53] | Butt join | 5.0 | 1000–6000 | 50 | -0.35-0.35 |
| Pure Al, mild steel [27] | Lap joint | 1.2 | 1002–2502 | 198–300 | – |
| 5083 Al, ST12 mild steel [20] | Lap joint | Al 3, steel 1 | 750–1125 | 70–230 | – |
| Pure Al, stainless steel [42] | Lap joint | Al 2.2, steel 1.1 | 950 | 60–375 | – |
| 6063 Al, HIF-GA Zn coated steel [51] | Lap joint | Al 3, steel 1 | 700–1500 | 30–100 | – |
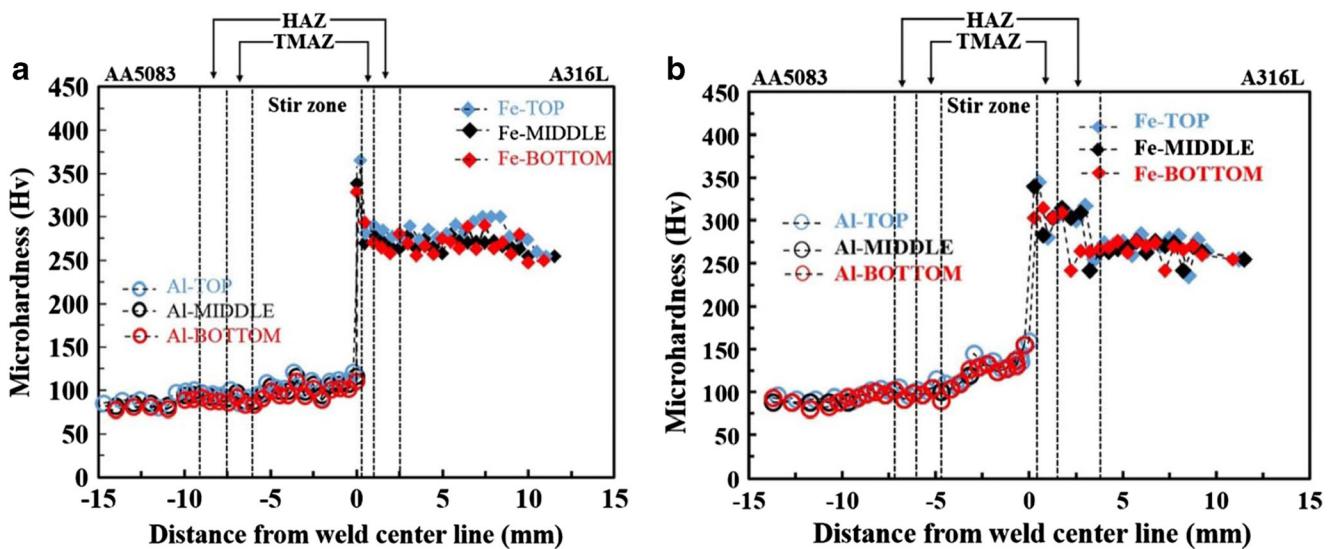
Fig. 11 Micro-hardness profiles across the joint interface of dissimilar Al/steel joints with different welding parameters [42]. **a** Rotation speed of 250 rpm, welding speed of 20 mm/min and **b** rotation speed of 250 rpm, welding speed of 16 mm/min. The base material and extends of HAZ, TMAZ, and SZ regions are marked

some voids were formed, resulting in the decrease of the joint strength. Fracture in the joint made with an offset of 1 mm occurred along a couple of paths. The IMCs formed at the upper region of the Al/Fe interface appeared to reduce the joint strength.

### 3.3.2 Lap joint

The fracture surfaces mainly consisted of two types of morphologies: brittle fracture, which was more prominent, and ductile fracture, which involved phases broken in a brittle manner. Many Fe-rich fragments stuck to the fractured surface of the Al side and the fracture occurred mainly along the layer

structure involving IMCs [45]. The welding parameters have important influences on the fracture locations of the Al/steel FSW joints. Table 4 showed failure regions of Al/steel FSLW joints with different welding parameters [70]. Failure occurred outside the weld zone and close to the shoulder periphery at lower welding speed. However, failure zone shifted toward retreating side in BM as the welding speed was increased. It suggested that the welded region did not have greater strength than the BM. The failure region shifted toward the BM, leading to the increase of maximum tensile strength. The multipass FSW strategy was also applied to increase the bonding area for improving the joint strength [58]. The occurrence of wavy interface and small discontinuities led to the difference of the
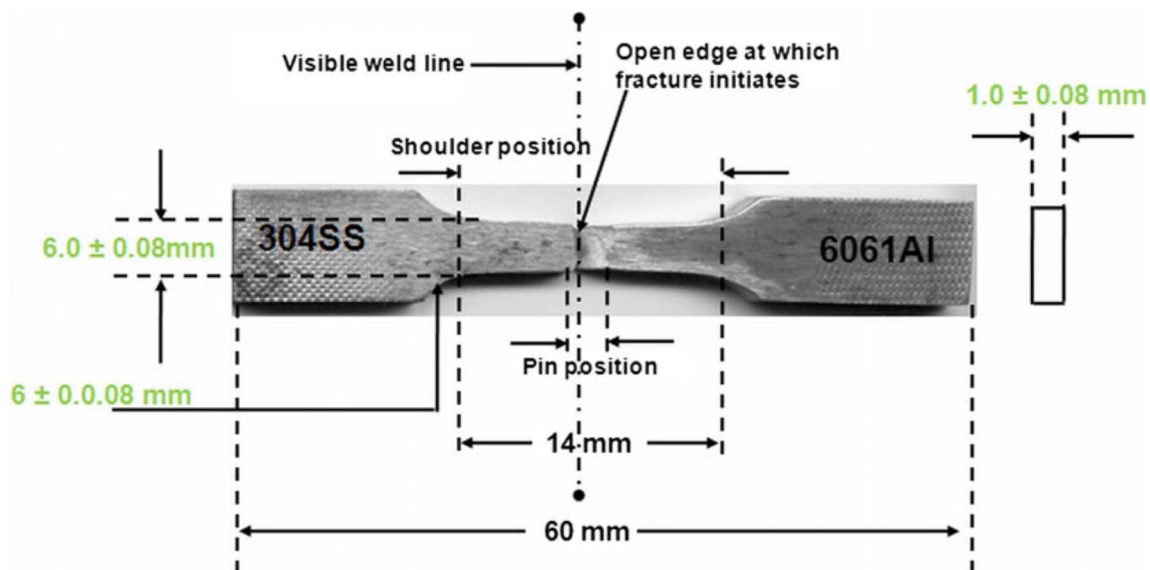


Fig. 12 Tensile-tested broken dissimilar weld showing the fracture initiation location and relative position of the tool with respect to the parallel length (not to scale) [51]

**Fig. 13** Effects of a pin offset on the microstructure and fracture path of welds [7]



Offset of a pin
(a):-0.2mm, (b):0mm
(c):0.2mm, (d):0.4mm
(e):0.6mm, (f):1.0mm
(g):2.0mm
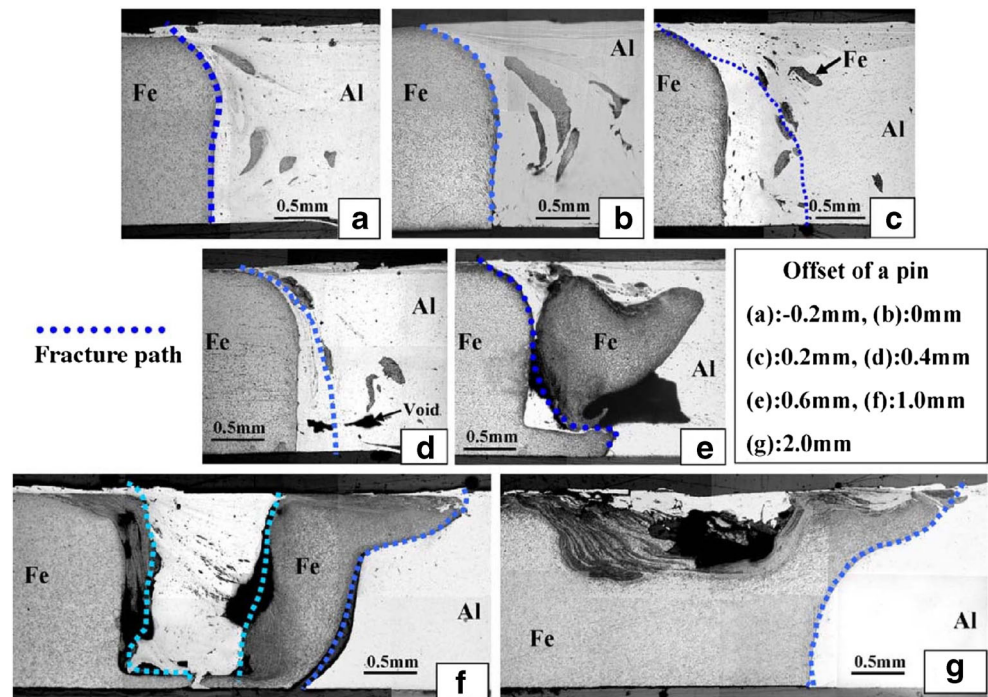
Fracture path

fracture path compared to conventional FSLW joint. Digital image correlation method was developed to acquire strain distribution maps during tensile test, as shown in Fig. 14. The tensile shear behavior demonstrated the non-uniformity of the bonding between the different weld passes. The engineer can improve weld performance by insuring the continuity of the bonding.

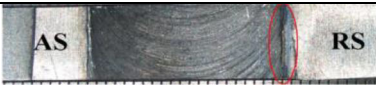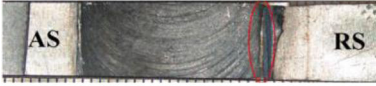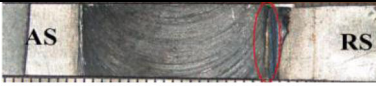# 4 Weld formation, macro- and microstructure
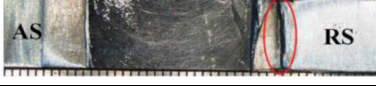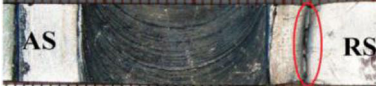
## 4.1 Butt joint

Figure 15 showed cross-sectional morphologies of typical Al/ steel friction stir welded butt joints. The cross sections of the joints could not be properly partitioned according to some characteristics or rules, especially the dividing lines between TMAZ and HAZ were not obvious. Uzun et al. [9] friction stir welded dissimilar 6013-T4 aluminum alloy and X5CrNi18-10 stainless steel, and divided the joint into seven distinct regions, as shown in Fig. 15a. The stir zones at the aluminum side exhibited composite structure in which an aluminum matrix containing steel particles was pulled away due to stirring and forging action of the adjacent A316L stainless steel base metal at the interface. Steel particles aligned themselves into the material flow direction with various sizes in different shapes. Large steel fragments and tiny platelets, which were sheared off from the steel plate due to abrasion and scraping action of the rotating tool, were distinguishable in the microstructures. No continuous IMC layer was seen at the Al/steel bonding

interfaces, but some tiny discontinuous IMC layers with average size less than 0.5 μm was seen at the high-magnification image of the interface. Figure 15b showed the optical macrostructure of the joint made from austenitic stainless steel and aluminum alloy [10]. Because the welding tool was shifted toward the aluminum alloy side, the stirred zone was mainly formed on the aluminum alloy side. Broken stainless steel particles escaping from the butted surface were distributed within the SZ. The SZ had a structure resembling that of a stainless steel particle reinforced Al alloy. When the soft material was placed on the retreating side, the interface span was larger, and when the hard material was placed on the retreating side, the interface span was smaller. Placement of the tool pin also played an important role in material flow and intermixing. The welded regions showed alternative gray and dark banded structures which contained different intermetallic particles due to material mixing. A good amount of material mixing was noticed without tool offset. With tool offset to the steel side, less material mixing with reduced banded structure was observed. With tool offset to the aluminum alloy side, least material mixing was observed with no obvious banded structure formation. The differences in material mixing and band structure with respect to the tool offset were likely related to the frictional heat generation and local composition variation.

### 4.1.1 Macroscopic overview of the cross section

Frictional heat input dominated by tool rotation speed, welding speed, and tool geometry influences the weld integrity. Derazkola et al. [90] compared cross sections and

**Table 4**   Fracture zone occurred in different welding parametric combination [70]

| Experiment no. | Welding speeds (mm/min) | Tool PD (mm) | Welded specimen after UTS |
|---|---|---|---|
| 1 | 31.5 | 0.1 | |
| 2 | 31.5 | 0.2 | |
| 3 | 31.5 | 0.3 | |
| 4 | 63 | 0.1 | |
| 5 | 63 | 0.2 | |
| 6 | 63 | 0.3 | |
| 7 | 125 | 0.1 | Al and steel sample got separated at the interface, for all samples at different overlapping lengths. |
| 8 | 125 | 0.2 | |
| 9 | 125 | 0.3 | |

macrostructures of FSW butt joints of AA1100 aluminum alloy to A441 AISI steel using four different welding parameters. When the heat input was lower, the long worm hole was formed in the aluminum side due to improper heat flux. By increasing the tool rotation speed, the defects disappeared due to higher frictional heat. Further increasing heat input and stir action of the tool shoulder, the plastic deformed steel was stretched into aluminum alloy and steel fragments separated in the stir zone at the aluminum alloy side. Further increase in the heat input promoted a larger mixed zone with the presence of increased amount of IMC structure and a crack propagating along the mixed patterns. Tool plunge depth also played a



**Fig. 14** Load-displacement graph and strain distribution maps acquired during monotonic shear-tensile tests [58]
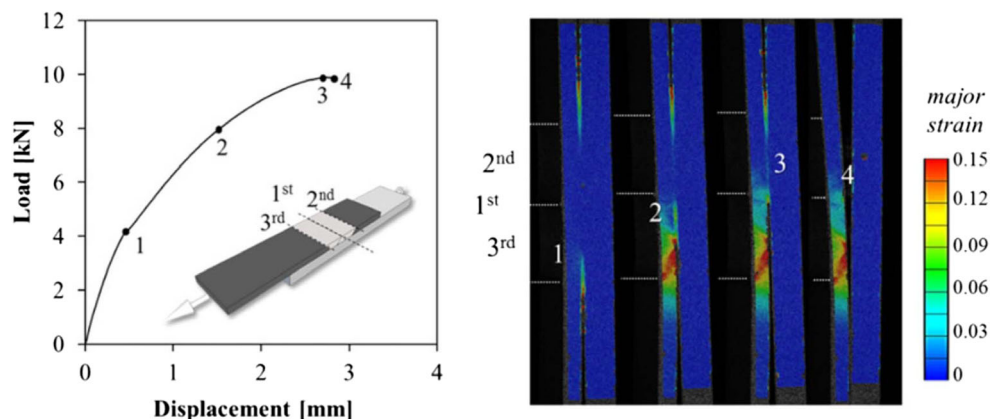
**Fig. 15** Macroscopic overview of the cross-section of the Al/steel FSW joints. **a** 6013-T4 aluminum alloy to X5CrNi18-10 stainless steel [9], and **b** 6065 aluminum alloy to 304 stainless steel [10]
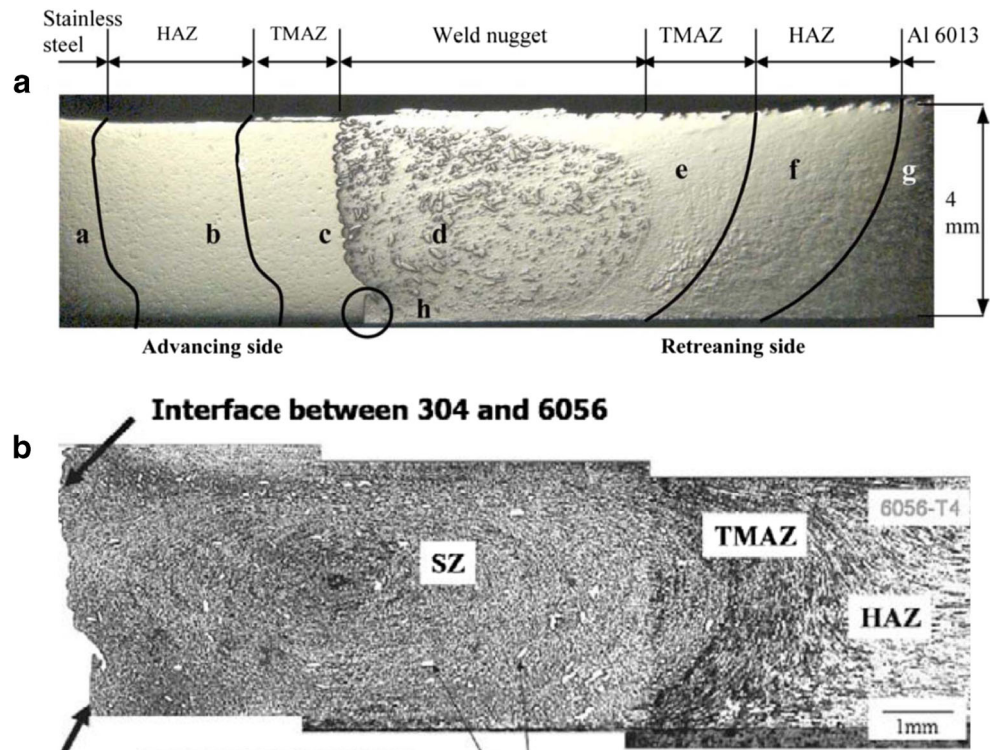


predominant role, which had direct impacts on heat generation and amount of friction. Tool plunging referred to welding pressure and axial force, which caused changes in total heat generation. Figure 16 showed the macrostructure of the cross sections of the joints with different tool plunge depths. The 0.1-mm tool plunge depth caused poor material mixing, incomplete superficial flow, and emergence of crevice inside the joint, resulting in the decrease of the ultimate tensile strength. With increasing plunge depth to 0.2 mm, material flow and interlace became more, and mixing degree of materials increased. By increasing tool plunge depth up to 0.4 mm, axial force and downward forging force increased, it increased stir zone squeezing. Therefore, hot metal stuck on the shoulder surface, as shown in Fig. 16c. Over necessitous axial force in 0.4 mm plunge depth caused the dislodge materials from the joint zone and made many defects in stir zone. When the plunge depth was equal to 0.6 mm, excessive axial force was produced. Large chunks of steel and aluminum were visible in the cross-section of the joint, representing the excessive downward forging force and sticking of materials (Fig. 16d). This excessive force led to the formation of unsound joint and produced narrow crack and tiny holes.

### 4.1.2 Microstructure characteristics of the WNZ

The microstructure of the WNZ of Al/steel FSW joints was characterized by disorder and inhomogeneity [41, 93], as shown in Fig. 17a. In view of its morphology, distribution, and composition, it was divided into three types including continuous parent material, layered structure (Fig. 17b, c), and dispersed particle composite structure (Fig. 17d). The curling and vortex layered microstructure was observed in local region of the WNZ. The closer the nugget zone was, the more obvious the laminated structure was. The plastic deformed steel in retreating side was flowed into the WNZ, broken, and then mixed with the aluminum matrix due to the severe friction and stir function of the rotating tool, as shown in Fig. 17. The broken steel particles distributed in the matrix [7, 81] reacted with plastic deformed aluminum alloy and formed stainless steel particles reinforced aluminum alloy [9], mechanical alloying organization [63], and so on.

### 4.1.3 Interfacial feature

The interfacial region of Al/steel FSW joint undergoes complicated plastic deformation process along with the high heat input and is easy to produce submicron stacked structure which is related to the atom diffusion. Lee et al. [10] studied the reaction layers of Al/steel FSW joints consisted of mixed layers of elongated and ultra-fine grains and the IMC layer, as shown in Fig. 18. From the EDS analysis, points 2 and 4 which were related to the lighter region were found to be mainly composed of stainless steel elements, while a very small amount of element Al was also detected. The lighter region in the mixed layer was identified as the deformed or flowed stainless steel part, including Al atoms diffused from the Al alloy. Point 3, which was related to the darker region,
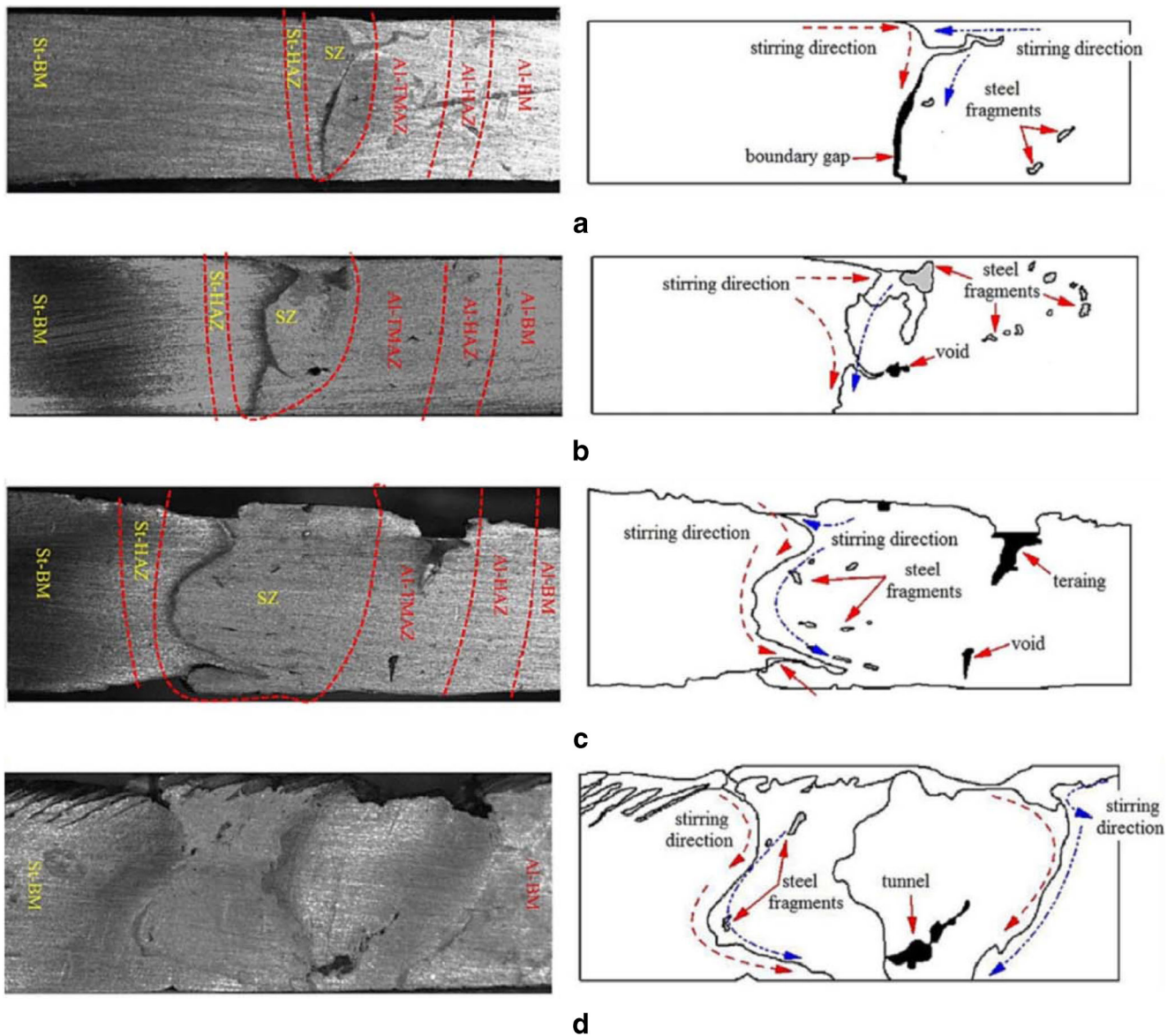
**Fig. 16** The macrostructure of the cross-sections of the Al/steel FSW butt joints with different tool plunge depth [90]. **a** 0.1 mm, **b** 0.2 mm, **c** 0.4 mm, and **d** 0.6 mm

was mainly composed of Al and some Fe, Cr, Ni, and Cu. The EDS results confirmed that this layer consisted of deformed aluminum alloy along with diffused stainless steel elements. In the region between the mixed layer and the recrystallized aluminum alloy, a continuous layer with a thickness of less than 1 μm was formed.

## 4.2 Lap joints

### 4.2.1 Macroscopic overview of the cross section

The interfacial macrostructure of the Al/steel lap joint presents two different forms according to plunge depth of the stir pin into or not into the steel surface. Aluminum alloy and steel are joined through some kind of mechanical joining, and the joining region is only under the domain of the probe diameter. When the stir pin is pressed into the steel surface, hook-like structure will be formed in both the advancing side and retreating side. Figure 19b showed the zigzag appearance at the longitudinal section of the WNZ in the interfacial zone [94]. Under the combined functions of friction and stir of the rotating tool, the plastic deformed aluminum alloy rotated with the tool and the plastic deformed steel flowed up into the aluminum alloy WNZ. The mixed Al/steel flowed into the trailing side to fill the cavity left by the tool movement and form the zigzag appearance. When the stir pin was not pressed into the steel surface, the interface was flat and uniform [95], as shown in Fig. 19d.

**Fig. 17** Typical microstructure characteristics of Al/steel FSW joints. **a** A magnified view of the WNZ [93], **b** layered structure in 5083Al/ss400 steel joint [81], **c** layered structure in 6061Al/AISI1018 steel joint [8], and **d** particle structure [9]
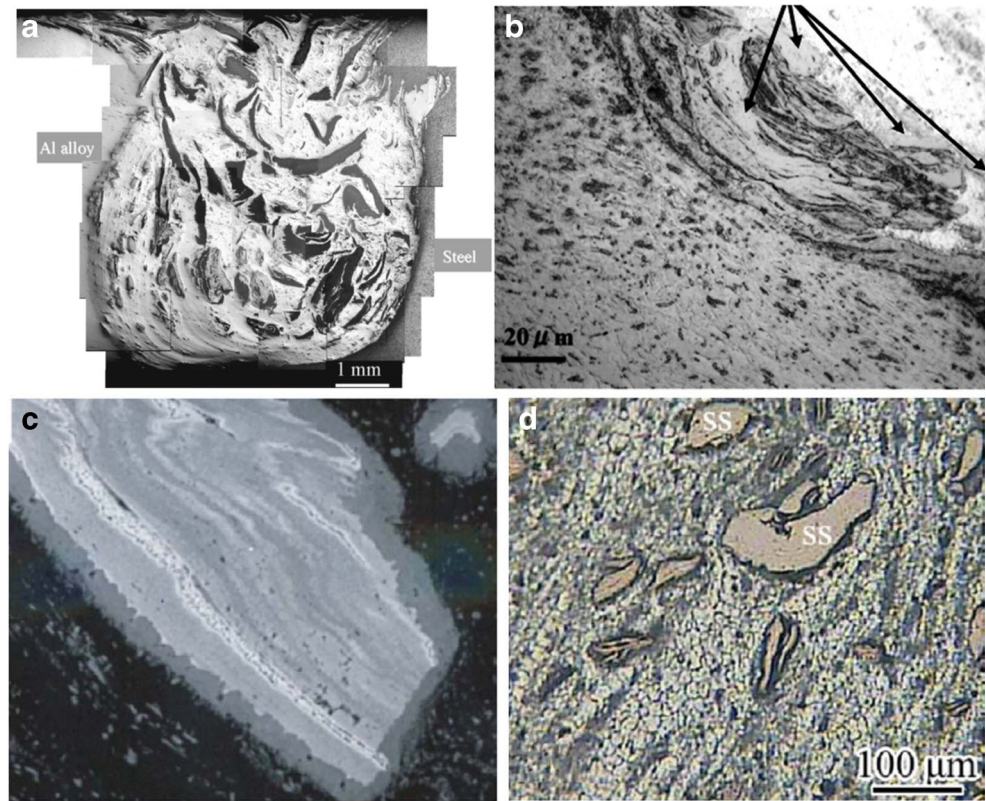


### 4.2.2 Microstructure characteristics of the WNZ

Figure 20 showed striated regions of texture through the WNZ at the top of the interface of Al/steel joint [72]. The striated structures were the product of the morphology of both the pin tip at the weld interface and the flow of material around the pin threads further from the weld interface. There existed three distinct layers of texture, as shown in Fig. 20d. The material directly below the tip of the pin experiences both shearing and compression deformation. The polar figures showed shear texture fibers with varying levels of rotation between the layers. The intensity of the peaks in the polar figure in (a) was more than double the intensity in (c). Like the WNZ in the aluminum alloy side, the steel WNZ also showed layers of
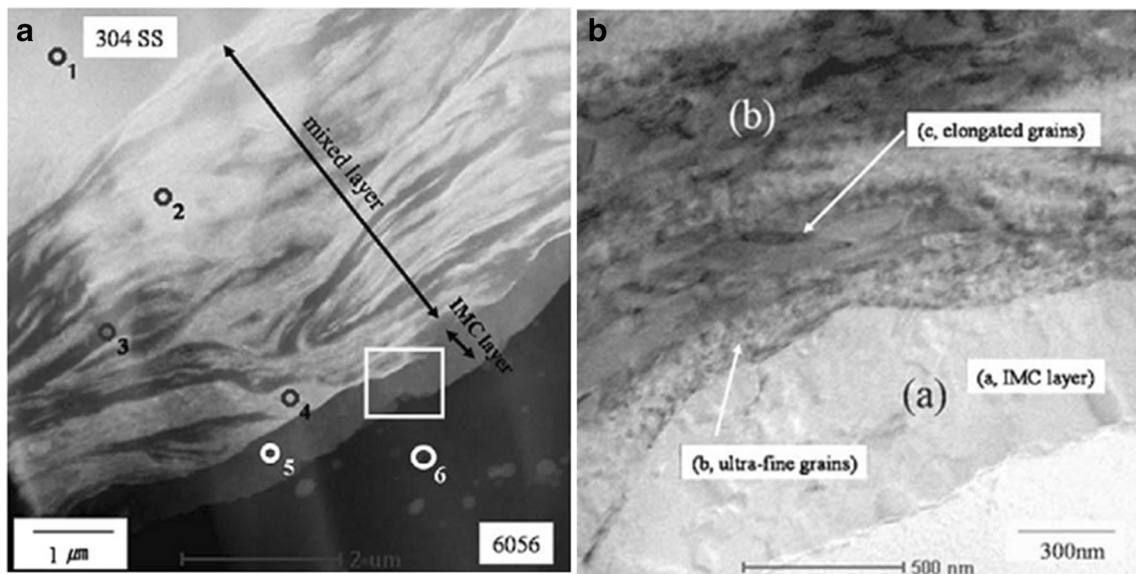


**Fig. 18** Interfacial microstructure of 6056Al/ss304 FSW joint [10]. **a** TEM micrograph of the interfacial region and **b** mixed layer and intermetallic compound layer
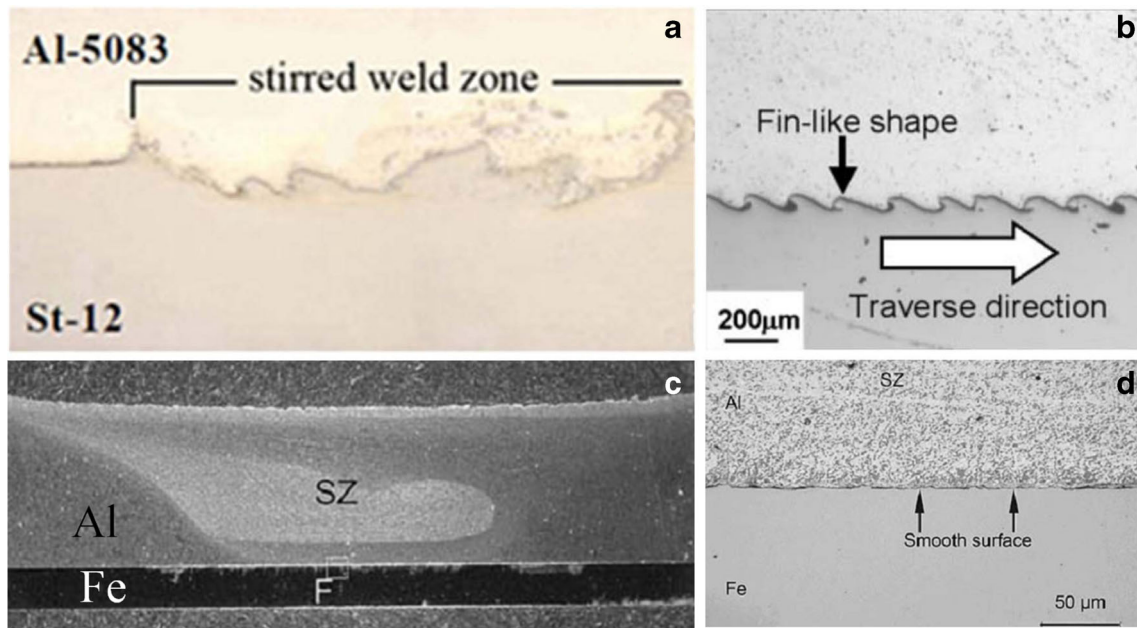
Fig. 19 The comparisons of the cross and longitudinal sections of Al/ steel FSLW joints. **a** The cross section of the joint with stir pin into steel surface, **b** the longitudinal section of the joint with stir pin into steel surface [94], **c** the cross section of the joint with stir pin not into steel surface [95], and **d** the longitudinal section of the joint with stir pin not into steel surface [94]

different textures accompanied by changes in grain shape, as was seen in the orientation map and polar figures in Fig. 20b, c. As distance from the weld interface increased, the shear texture components became less identifiable.

### 4.2.3 Interfacial feature

The interfacial microstructure of the Al/steel lap joint also presents two different forms according to plunge depth of the stir
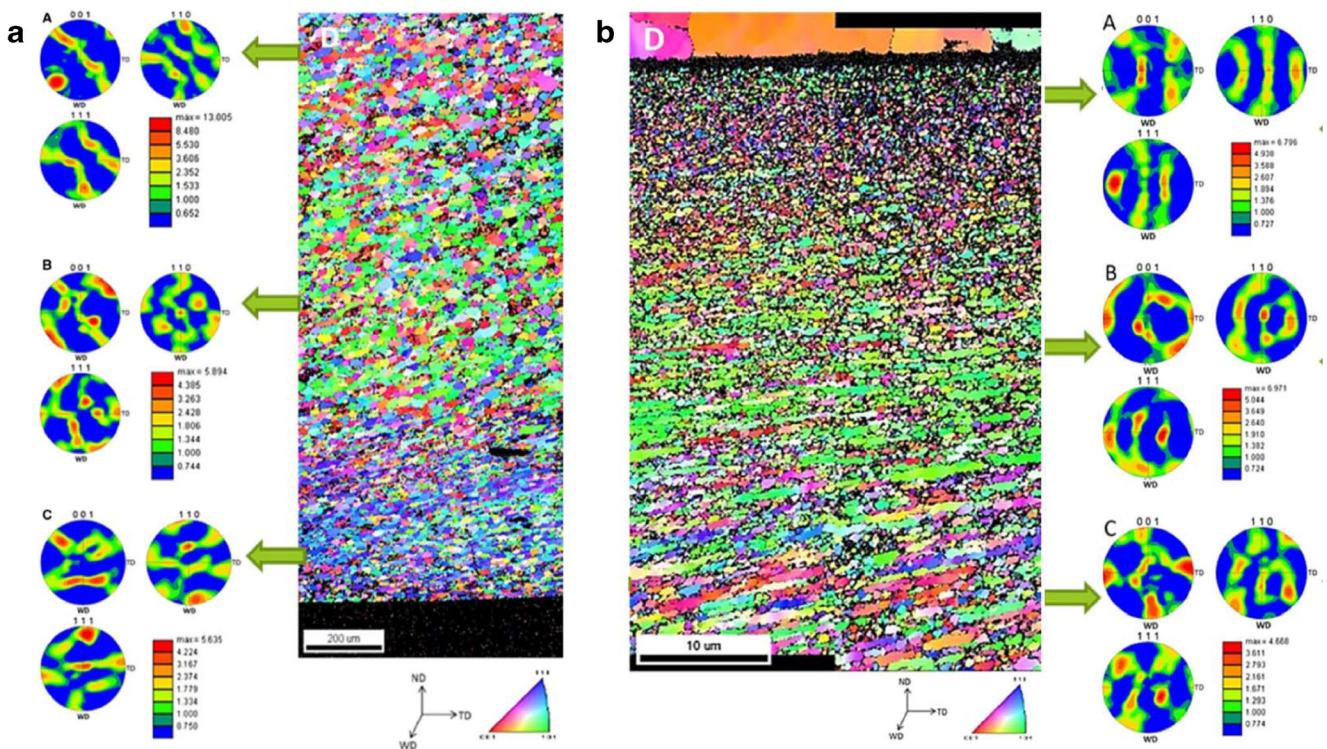


Fig. 20 **a** 6061-T6 WNZ center showing layers of differing textures and **b** striated layers of texture and grain size in steel WNZ center [72]

pin into the steel surface. When the stir pin is pressed into the steel surface, the interfacial microstructure of Al/steel lap joints is characterized by disorder and inhomogeneity. In view of its morphology and composition, it was divided into continuous parent material and layered structure, as shown in Fig. 21. The curling and vortex-layered microstructure was observed in local region of the WNZ. The closer the nugget zone was, the more obvious the laminated structure was. When the stir pin was not pressed into the steel surface, the interfacial microstructure was flat and smooth. Under normal conditions, the maximum temperature of the WNZ would not exceed the melting point of the aluminum alloy BM. However, the maximum temperature in some special region maybe reach or even exceed eutectic temperatures of two components [96], leading to the low melting eutectic phenomenon in WNZ, as shown in Fig. 21c, d.

Chen and Nakata [95] friction stir lap welded AC4C Al alloy (top sheet) and steel with three different kinds of surface state including zinc-coated steel, brushed finish steel, and mirror finish steel. The lap joints were produced when the FSLW tool did not touch the lower steel surface. Figure 22a showed that the joint consisted of a mixed structure including an IMC layer and a residual zinc layer. Aluminum alloy and steel were joined through the intermediate reaction zone. During FSLW

process, the metal in the lap interface underwent the synthetic effect of the thermal cycle and the mechanical cycle. High temperature led to the melting of the zinc coat, and high pressure simultaneously resulted in the rupture of surface oxide films, which promoted the formation of low-melting Al-Zn eutectic reaction products. High pressure extrudes the liquid phase of Al-Zn eutectic reaction product, which spread along the interface. In this way, the fresh interfaces of Al and the residual zinc layer were exposed, and they were tightly extruded together. Mutual diffusion of aluminum and iron occurred in elements, which led to the formation of a new IMC layer adjacent to the lap interface. Figure 22b showed the microstructure of the region far from the WNZ but still under the shoulder. The mixed structure was still present. Figure 22c showed the microstructure of the region in which aluminum alloy and zinc-coated steel were in unbound state. A typical eutectic structure was found and filled into the clearance. Figure 22d, e showed microstructural variations at the lap interface of aluminum and brushed finish steel. No significant IMC layer was found at the interface in WNZ. Aluminum alloy was pushed into the concavities of the brushed finish steel surface. The base materials were joined through some kind of mechanical joining. However, AC4C aluminum and
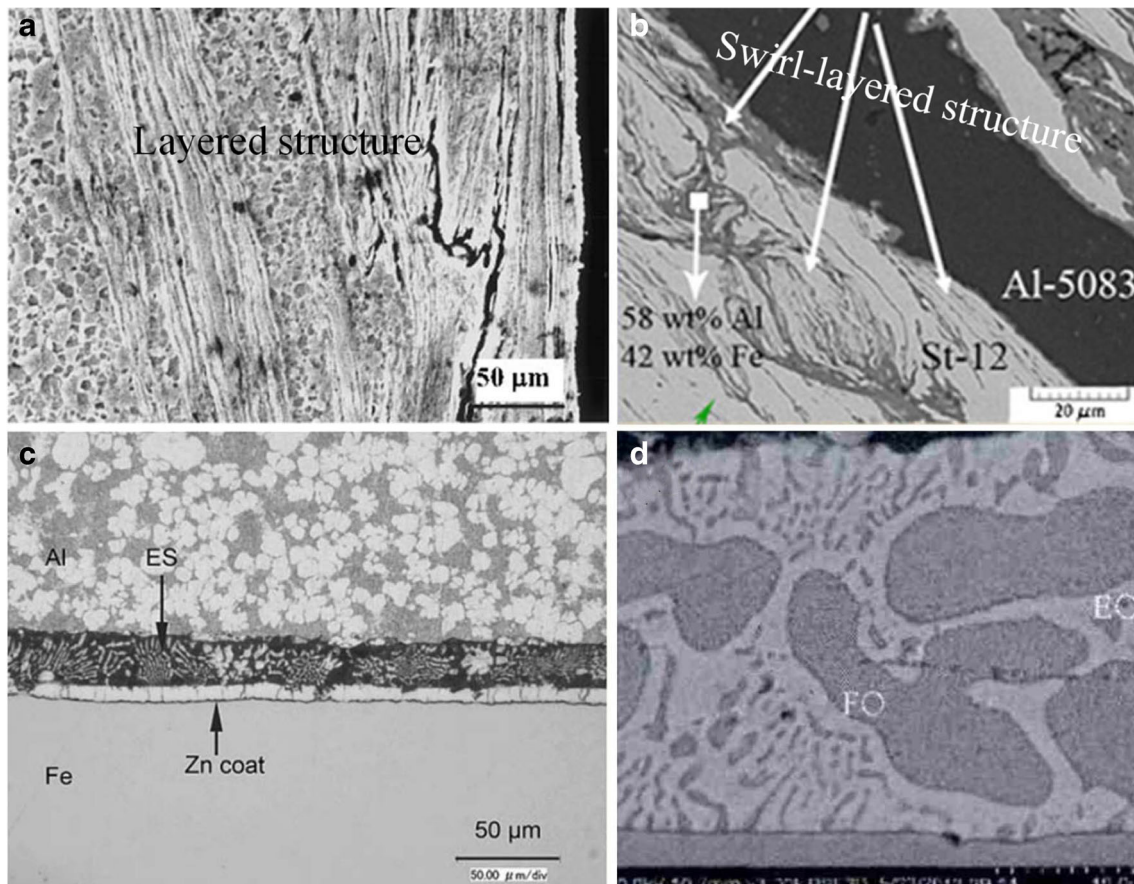


**Fig. 21** Typical microstructure characteristics of Al/steel FSLW joints. **a** Layered structure [45], **b** swirl-layered structure [30], **c** the eutectic structure fills into the clearance between aluminum alloy and zinc-coated steel [96], and **d** typical eutectic structure [96]

**Fig. 22** Effect of the surface state of steel on the interfacial microstructure of dissimilar Al/steel FSLW joints [95]
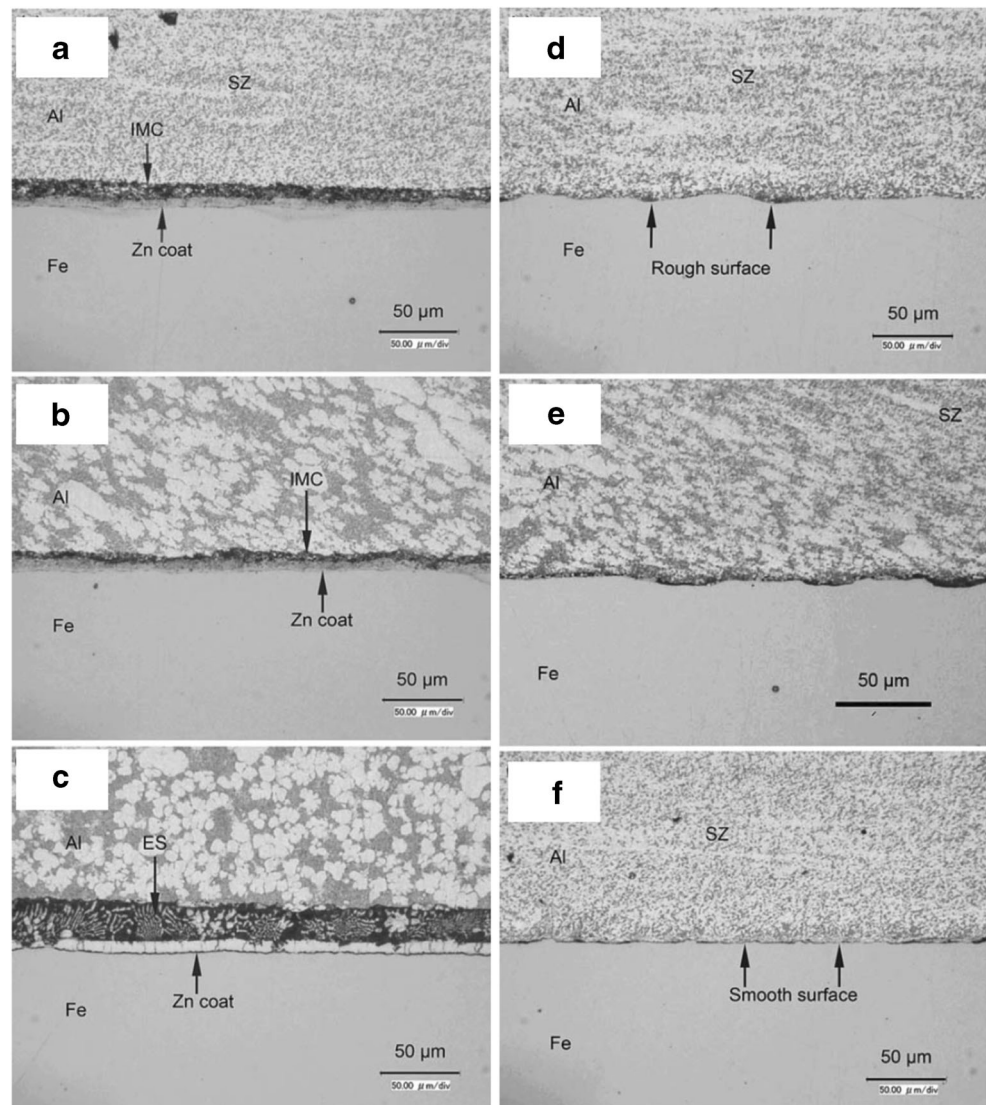


# 5 Metallurgical bonding of Al/steel FSW joints

## 5.1 Typical types of interfacial structures

Among available researches on FSW of aluminum alloys to steels, regardless of the use of various alloy systems, welding parameters, or configurations, one common feature is the formation of IMC at the interface between Al and steel alloys. The thickness of IMC layer increases with the increase of heat input during the FSW process. However, the lower heat input and higher welding speed will easily lead to the discontinuity of plastic material flow, resulting in the incomplete interface. Meanwhile, if the offset or depth of stir pin into steel side is high, the interfacial defects will form due to the discontinuity of plastic material flow, and the wear of the welding tools will become serious [6]. The interfacial reaction and composition of Al/steel FSW joints were complicated, consisting of swirl or vortex-like intercalation structure and IMC layer [10]. It can be seen that the joint performance is closely related to the interfacial structure. The formations of IMCs (Fig. 23a), interfacial reinforced composite, or amorphous layer (Fig. 23b) at the interface depended on the heat input and the degree of plastic deformation, which had great influences on joint properties. The effect of the stirring action and high strain rate on the stainless steel part after the FSW partially contributed to the ferrite transformation from the austenite phase even at a relatively low temperature, as shown in Fig. 23c. Owing to interdiffusion of chemical species across the bond line, discrete
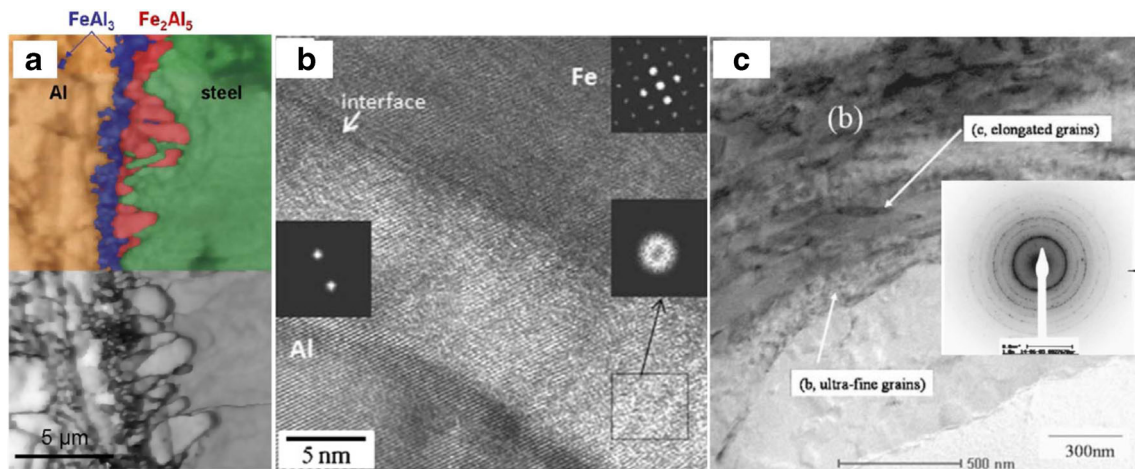
mirror finish steel could not be welded at the same parameters. Figure 22f showed the smooth surface of the mirror finish steel. It could be concluded that the low melting eutectic phenomenon promoted the interdiffusion of Fe element and Al element and the surface state of the steel affected the joint quality.

**Fig. 23** The complicated interfacial reaction of Al/steel FSW joints. **a** The presence of two IMCs at the interface: face-centered cubic Al in orange, monoclinic FeAl$_3$ in blue, orthorhombic Fe$_2$Al$_5$ in red, and body-centered cubic Fe in green [83], **b** an amorphous structure [76], and **c** the hypothesized phase transformation from austenite phase to ferrite phase [10]

islands of Fe$_3$Al intermetallic phase formed within the diffusion zone, contributing to the improvement of joint strength [14]. The weld nugget was considered as aluminum matrix composite, which was enhanced by dispersed sheared-off steel fragments encompassed by a thin intermetallic layer or simply intermetallic particles [52]. The formation of an amorphous structure near the Al/Fe interface revealed that a non-equilibrium phase was formed due to the mechanical alloying during the severe plastic deformation, but not the thermally driven mechanism. The formation of an amorphous structure in the binary Al-Fe alloy system was only formed with a chemical composition beyond the solid solution limitation, as shown in Fig. 23b. Moreover, the super saturation solid solute was generally obtained through mechanical alloying at a low temperature [76]. Otherwise, IMC would be formed due to their thermodynamic priority at high temperature.

## 5.2 The formation of IMC layer

The formation of the IMC is the main factor influencing the properties of Al/steel joint, and the thickness of which has a critical value. The mechanical properties of joints could be improved when the thickness of IMCs at the Al/steel interface

was less than the critical value; otherwise, the crack was easy to initiate and expand at the interface, which made the bearing performance of the joints become deterioration. Table 5 showed the types and critical thickness of IMCs in previous studies. The continuous thin reaction layer with thickness of 100–150 nm produced at the interface contributed to the joining between the aluminum alloy and stainless steel, and was found to be stronger than the base aluminum alloy [100]. The IMC layer of FeAl or Fe$_3$Al with thickness of less than 1 μm was formed at the Al/Fe interface in the advancing side, which could actually contribute to the joint strength [52]. Tanaka et al. [6] found that the joint strength increased with reduction in thickness of the IMC at the weld interface. Figure 24 showed that the thickness of the IMC strongly influenced fracture point of the joints. With the exception of the joints in the AA7075 aluminum alloy, all the other welds, with thin IMC layers, failed in the aluminum alloy BM.

The existence of Fe-Al IMC at the interface plays two different roles on joint properties. On the one hand, the existence of IMC layer indicated the metallurgical bonding between aluminum alloys and steels, resulting in the improvement of welding quality [101], as shown in Fig. 25. On the other hand, the presence of excessive IMC layer caused stress

**Table 5** The types and critical thickness of IMCs in previous studies

| Base materials | Types of IMCs | Critical thickness of IMC | References |
| --- | --- | --- | --- |
| TRIP steel and Al 6061 | FeAl and Fe$_3$Al | 1.0 μm | [52] |
| St-12 alloy and Al 5083 | FeAl$_3$ | 2.0 μm | [30] |
| Ultralow carbon steel and Al 1050 | FeAl$_3$ and Fe$_2$Al$_5$ | 2.5 μm | [83] |
| St-12 alloy and Al 5083 | FeAl$_3$ and Fe$_2$Al$_5$ | 2.6 μm | [97] |
| HIF-GA steel and Al 6061 | Fe$_4$Al$_{13}$ | 6.5 μm | [98] |
| IF-steel and Al6016 | FeAl$_3$ | 8.0 μm | [63] |
| 1050 and mild steel | – | 10.0 μm | [99] |
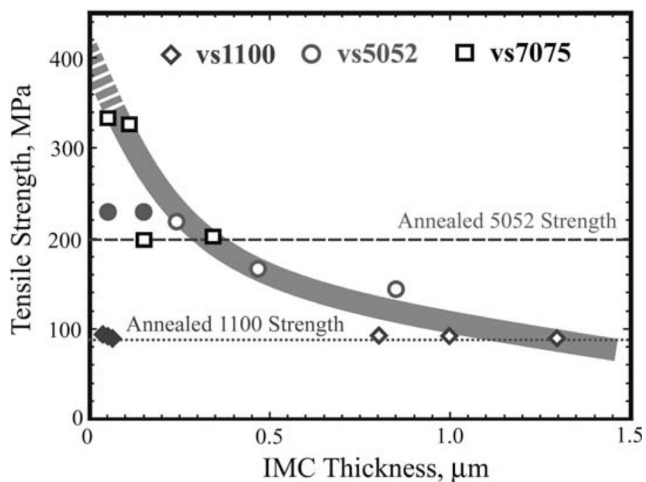
**Fig. 24** Relationship between joint tensile strength and IMC thickness for Al/steel welds [6]

concentration due to the change of the phase volume, and deteriorated the bearing capacity of the joint. Some researchers had noted that thin IMC layers and Fe-rich IMCs were not detrimental to the strength of the joints and also improved the mechanical properties [76]. On the other hand, some studies indicated that thin IMC layers were responsible for the deterioration of joint properties [11, 45, 46, 56, 97]. Therefore, IMCs have different effects on the mechanical properties of the joints. The joints will achieve better performance when the thickness of IMC layer is in a certain range. The prevention of the IMC formation is important. Although it was reported that the formation of a narrow IMC layer along the interface may increase the mechanical properties of the dissimilar welds, the control of the layer thickness was difficult and an increase in the layer thickness would result in the crack formation and significantly decrease the mechanical properties [102].

The types of IMC phases also have important influence on the joint quality and Fe-rich IMC phases such as FeAl and $Fe_3Al$ have better toughness than Al-rich IMC phases like $Fe_2Al_5$ and $FeAl_3$ [33]. IMCs such as $FeAl_6$ [89], $Fe_4Al_{13}$ [8, 45], $FeAl_3$ [6, 7, 63, 79], $FeAl_4$ [10], $Fe_2Al_5$ [11], $FeAl_2$ [63, 79], FeAl [7], and $Fe_3Al$ [11] have been reported. TEM revealed $FeAl_4$ nano-layers [10], $Fe_2Al_5$, $FeAl_2$, $FeAl_3$ crystals [11], $Fe_2Al_5$ layers with nano $FeAl_3$ islands [103], and nano $Fe_2Al_5$, $FeAl_2$, $FeAl_3$ intermetallics [76, 104] at the interface of Al/steel joints. Abbasi et al. [105] investigated Fe-rich fragments and surrounding IMCs in Al/steel FSW joint and Fig. 26 indicated that the fragments were covered by a layer of orthorhombic $Fe_2Al_5$, which was surrounded by a mixed region composed of sub-micrometer $FeAl_3$ crystals in a matrix of Al nano grains. Fe content was decreasing away from the fragment. Meanwhile, Al content exhibited an increasing trend approaching the aluminum matrix. Haghshenas et al. [61] and Fei et al. [106] pointed out that the types of IMC phases had a great influence on the property of the Al/steel joint and the performance of the welds with Fe-rich IMC was better than that of the welds with Al-rich IMC.

## 5.3 The control of IMC layer

For FSW joints of dissimilar aluminum alloys and steels, one of the most important thing is how to control the amount of reactant. The thickness of reaction layer is a fundamental prerequisite to obtain welded joints with good performance. In the process of heterogeneous metals friction stir welding, the number of reactants is directly related to the kinetic problem and the rate of atomic diffusion. Beside the thickness of the IMCs, the type of IMCs also exerts significant influence on joint quality. It is reported that Fe-rich IMCs, like FeAl and $Fe_3Al$, were less brittle than Al-rich IMCs, like $FeAl_3$ [107]. It

**Fig. 25** HRTEM images of the interface of the FSLW joint of 3003 aluminum alloy and SUS304 steel [101]. **a** At the center region and **b** on the RS. The insets in (**a**) and (**b**) show the diffraction patterns for the corresponding regions
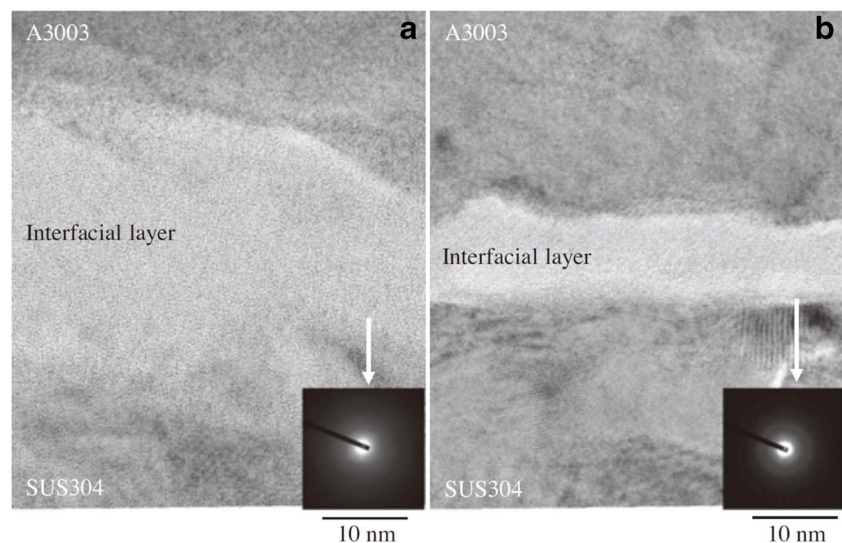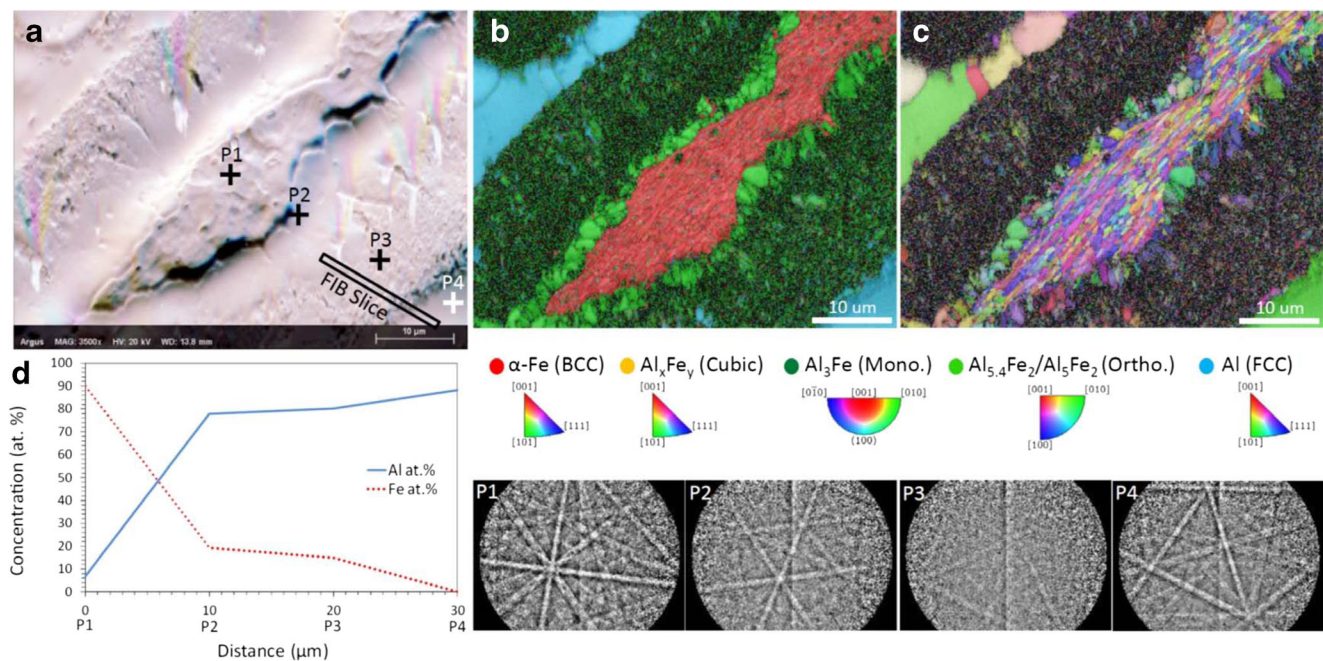
Fig. 26 **a** Higher magnification image illustrating post-etching surface topography of the Fe fragment and neighboring areas [105]. **b** EBSD + EDS phase map indicating the Fe fragment (red) covered by Al5.4Fe2/ Al5Fe2 orthorhombic phase (light green). **c** IPF map indicating fine elongated steel grains parallel to shear plane. **d** Atomic concentration of Al and Fe in points 1 to 4 (P1 to P4) in (**a**)

has been mentioned that the main concern is controlling the formation of the IMCs at the joint interface which is governed by the heat input controlling parameters including the tool rotation speed and welding speed. The heat generated by friction or material deformation mostly governs the generation of the IMC. Welding pressure and strain rate were other factors that controlled generation of IMC [108]. The higher rotation speed resulted in thicker IMCs because of the increased heat input created by friction and material deformation [6, 63, 109]. Liu et al. [52] revealed that high rotation speeds influence the composition of IMC layers and higher welding speeds reduced the IMC thickness because of the short high-temperature residence time. Furthermore, the variation of welding speed does not have any significant influence on heat distribution and IMC formation. Coelho et al. [4] reported that high shear strain and frictional heating during the process caused IMC formation. Bozzi et al. [63] found that an IMC layer with thickness of larger than 1 μm was formed between the Al and steel plate, and the formation of three kinds of IMC phases, $FeAl_3$, $Fe_2Al_5$, and $FeAl_2$, was identified depending on the different welding conditions.

## 5.4 Research status of atomic fast diffusion behavior

As an important material transfer phenomenon in metal research, atomic diffusion is the basic factor affecting the steady characteristics of materials, and one of the important methods to change the material structure in dynamic conditions. Atom diffusion is the only method of mass transport in solid state

and the smallest scale dynamic behavior in the evolution of material microstructure. The nature of the diffusion in solid is the oriented and macroscopic migration of the atoms under the influence of the diffusion force (the gradient of the concentration, electric field, stress and strain field). Once it changes obviously, the evolution of dislocation, grain boundary, and phase transition will also change. The change of the microstructure and the resulting change of the chemical and physical properties are closely related to the atomic diffusion in the metal material processing. Therefore, revealing the law of atomic diffusion in Al/steel FSW joint is of great importance for understanding and describing the evolution and formation of non-equilibrium microstructures.

### 5.4.1 The phenomenon of atomic fast diffusion behavior

Ma et al. [110] studied the friction stir process (FSP) of cast Al and Mg alloys, which resulted in the break-up of coarse dendrites and secondary phases, refinement of matrix grains, and dissolution of precipitates due to the severe plastic deformation. The high dislocation density introduced by severe plastic deformation resulted in the occurrence of pipe diffusion. The pipe diffusion rate was at least 1000 times higher than the bulk one for magnesium. Thus, for the same diffusion distance, the time needed for complete dissolution was shortened by at least 1000 times. Lap joining of a pure aluminum plate and a low carbon steel plate was performed using friction stir spot welding by Watanable et al. [111]. The thickness of the IMC layer increased with increasing the dwell time and was in

**Fig. 27** Back scattered electron images of the welding interface of the lap joint welded with each dwell time [111]
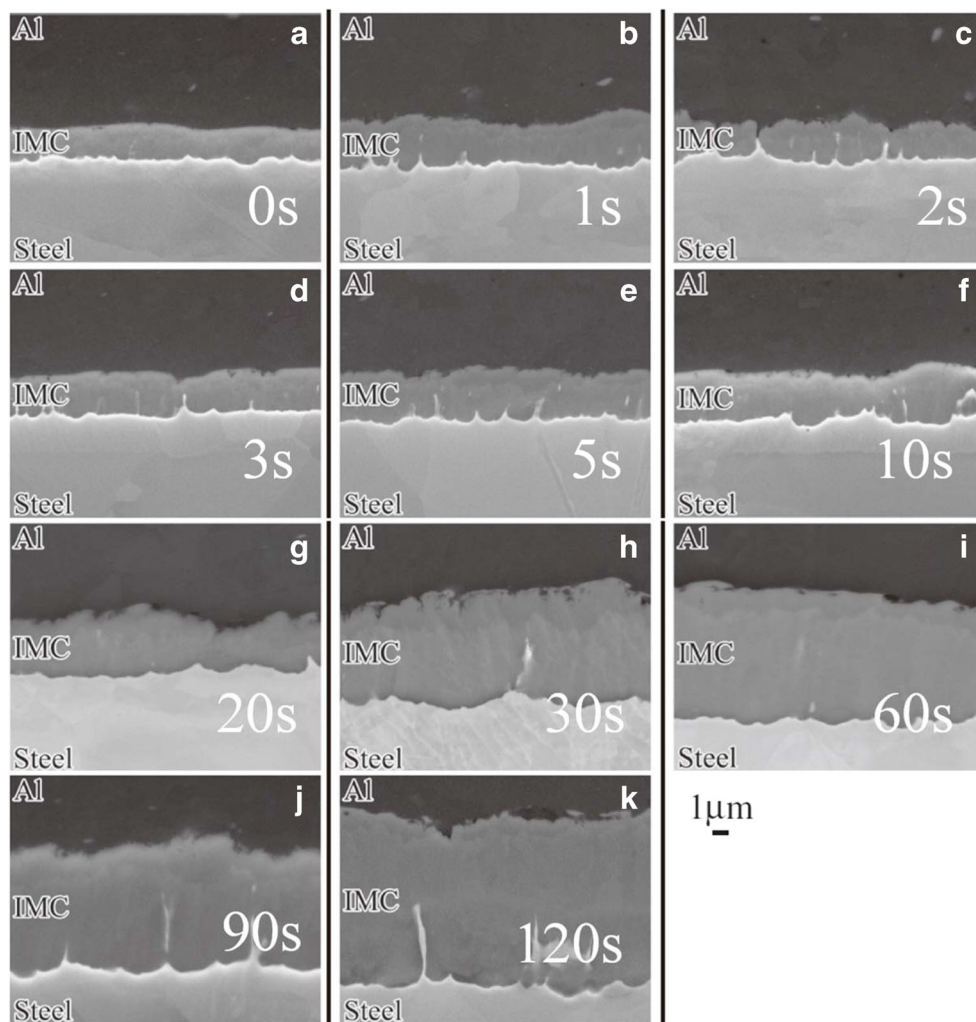


proportion to the square root of the dwell time, as shown in Fig. 27. The formation manner of the IMC phase was strongly affected by aspects of the welding process such as plastic flow, plastic deformation of the matrices close to the welding interface, and heating and cooling rates. The plastic flow resulted in crystal defects such as grain boundaries, dislocations, and vacancies, which enhanced the atomic diffusion and resulted in the pipe diffusion mechanism.

The refined grains formed in the surface layer of a bulk material can provide an effective approach to enhance the diffusion and chemical reaction kinetics. A large number of defective grain boundaries in nanostructured materials may act as fast atomic diffusion channels, hence greatly enhancing atomic diffusivities. Meanwhile, numerous grain boundaries in the nanostructured material also constitute a high stored energy that may facilitate the chemical reactions. The chemical reaction kinetics were observed to be greatly enhanced by the mechanical attrition treatment of solids, in which the grain size was significantly reduced to the nanometer scale and a large number of structural defects were created by the severe plastic deformation [112]. Figure 28 showed the existence of

the Al matrix and a high fraction of sub-micrometer elliptical second-phase crystals [105]. Presence of $FeAl_3$ crystals along low- and high-angle grain boundaries of Al implied that Fe diffusion was mainly responsible for their formation (Fig. 28b, d). Al grain boundaries offered fast diffusion paths for Fe atoms to reach low-Fe areas and nucleate $FeAl_3$ crystals. The area fraction of $FeAl_3$ crystals had increased from nearly 55% at the mixed zone/Al interface to more than 80% away from the interface (Fig. 28c).

No IMC layer but some areas with amorphous atomic configuration was formed along the Al/Fe joint interface due to the lower heat input. The formation of an amorphous structure near the Al/Fe interface revealed that a non-equilibrium phase was formed due to the mechanical alloying during the severe plastic deformation, but not the thermally driven mechanism. Fukumoto et al. [113] friction welded 304 stainless steel and 5052 aluminum alloy and observed that reaction layer of approximately 300 nm in thickness was formed. Interdiffusion of the elements occurred despite the short reaction time of 2 s. The crystalline phase and the amorphous phase were stacked alternately and the structure changed discontinuously at the
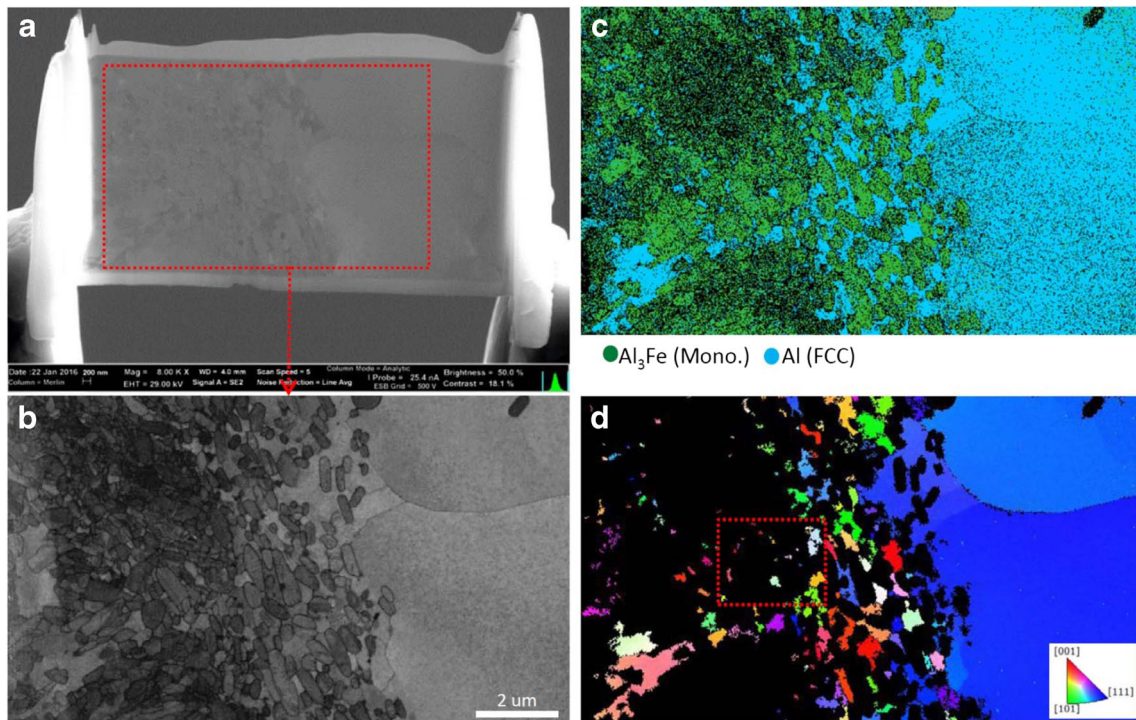
Fig. 28 **a** SEM image of the mixed region [105]. **b** Image quality map indicating ultrafine and nano grains in the mixed region. **c** Phase map indicating a high fraction of sub-micrometer monoclinic FeAl₃ (dark green) at the interface of aluminum (light blue) and the mixed region. **d** Orientation (IPF) map of Al indicating nano grains with a large orientation spread among FeAl₃

interface. The amorphization of the Al/Fe system at the interface was due to the complex mechanism of mechanical alloying and solid-state reaction processes following the hard rubbing at high temperature. Figure 29 showed an amorphous structure along Al/Fe interface [76]. The formation of an amorphous structure in the binary Al-Fe alloy system was only formed with a chemical composition beyond the solid solution limitation. Moreover, the super saturation solid solute was generally obtained through mechanical alloying at a low temperature [76, 114]. Otherwise, IMC would be formed due to their thermodynamic priority at high temperature. The phase transition from crystalline to amorphous phase must

be accompanied by mixing and rearrangement of atoms. The severe plastic deformation made both the grain and crystal lattice broken during the FSW process. The acquisition of fine grains may also be due to the crystallization of amorphous phase rather than the original grains. The atoms in amorphous phase were extremely chaotic, similar to that in liquid phase. Therefore, the corresponding atomic diffusion should be greatly different from that of atom under equilibrium state.

The existences of the IMC, solid solution, or amorphous phase can directly prove the existence of atoms diffusion phenomenon due to the severe plastic deformation during the FSW process. However, the reaction time is relatively short.

Fig. 29 **a** TEM and **b** high-resolution TEM showing microstructure along Al/Fe interface [76]
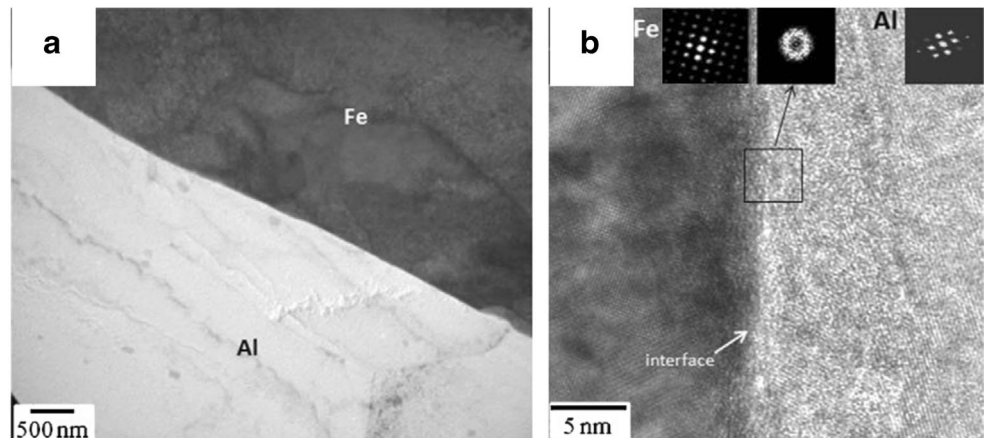
The actual joint formation time takes only a few seconds, and the longest is no more than 10 s. That is to say, atomic diffusion at the interface is accomplished in a very short time. Usually the thickness of IMC layer could reach 1–10 μm. FeAl and Fe₃Al with thicknesses of up to 93 μm were also reported by Pourali et al. [64]. It meant that the diffusion coefficient was large and the diffusion rate was very alarming corresponding to the short welding time. This could not be explained by classical thermal activation diffusion theory. Ghosh et al. [14] friction stir welded commercially pure Al and 304 stainless steel and found that diffusion of Fe, Cr, and Ni was substantial within Al; however, diffusion of Al within 304SS was limited. Owing to interdiffusion of chemical species across the bond line, discrete islands of Fe₃Al intermetallic formed within the reaction zone. The austenite underwent phase transformation to ferrite due to large strain within this grain. Tarasov et al. [115] studied diffusion wear mechanism in 1.2344 X40CrMoVS-1 steel FSW tool and found that the Fe/Al reaction diffusion was initiated under the conditions of high mechanical stress and temperature. Figure 30 showed different types of tribological layers on the FSW tool. The diffusion by the former austenite grain boundaries was much faster than volume diffusion where an IMC was formed inside the tool's metal. The formation of FeAl₃ IMC with hundreds

of micrometers by the grain boundary diffusion caused the grain boundary embrittlement and resulted in the voids inside the IMC formations according to the Kirkendall effect.

From the above phenomena, it can be summed up that the atoms in the contact interface undergo rapid diffusion during the friction and stirring process of FSW. This diffusion behavior is a thermal mechanical coupling process. The material itself influenced by the combined action of medium- and low-temperature thermal cycling and high-speed deformation behavior during the FSW process. The plastic deformed material near the FSW tool has higher atomic diffusion capacity and the higher strain rates are attributed to the diffusion process. It can be seen that the friction stir welding process is accompanied by the combined effects of plastic deformation and frictional heat. The state of thermal and mechanical coupling for the atomic diffusion is different from equilibrium states of classical atomic.

### 5.4.2 The proposal of super diffusion

In the diffusion process, the mean squared displacement $\sigma_r^2$ can be described as $\sigma_r^2 \sim Dt^\alpha$, where $D$ is the diffusion coefficient and $t$ is the diffusion time [116, 117]. In a typical
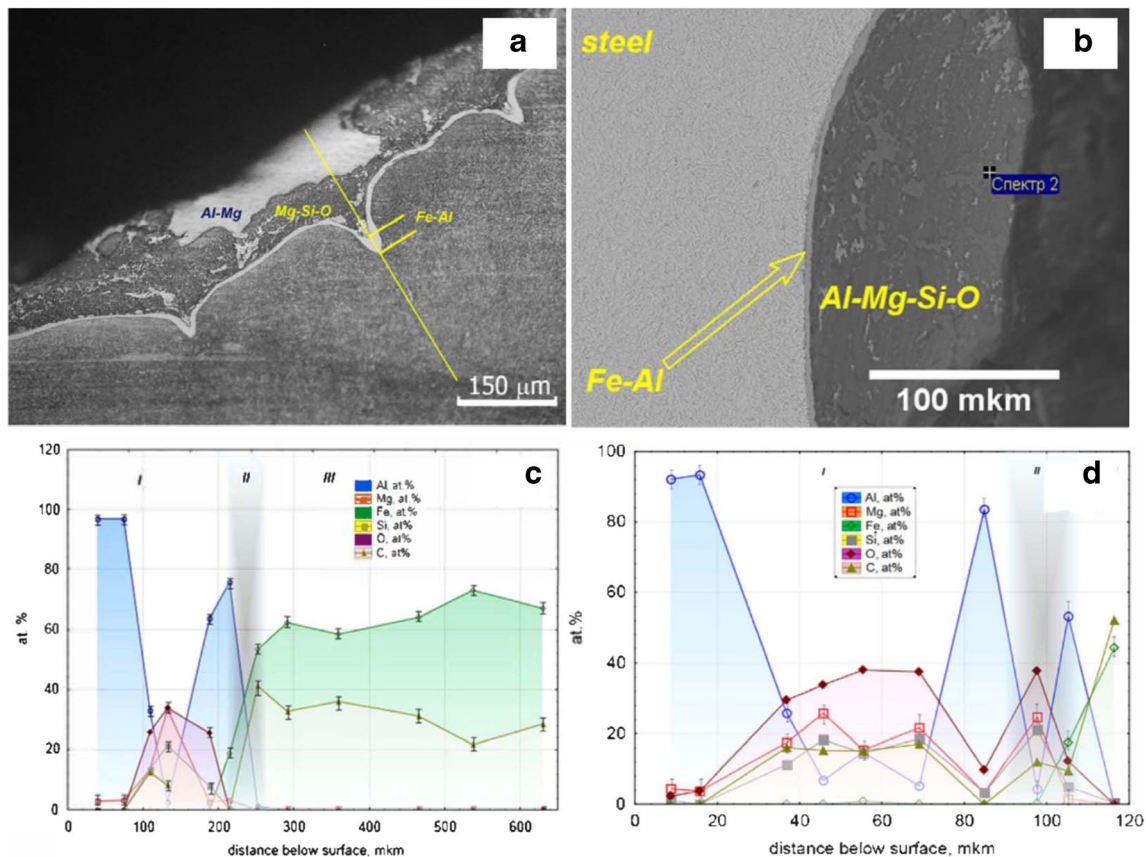


**Fig. 30** Different types of tribological layers on the FSW tool [115]. **a** Layer A, **b** layer B, **c** the EDX profiles of elements across the A layer, and **d** the EDX profiles of elements across the B layer

diffusion process, $\alpha = 1$ and $\sigma_r^2$ is a linear function of time. The classic atomic diffusion theory indicates that the nature of atomic diffusion is the thermal vibration of atoms and temperature significantly affects the diffusion coefficient. When the diffusion system is constant, the diffusion coefficient varies with the temperature index. Unlike typical diffusion, anomalous diffusion is described by a power law. If $\alpha > 1$, the phenomenon is called super diffusion. Super diffusion can be the result of active cellular transport processes. The atomic diffusion coefficient in the thermo-mechanical coupling process of friction stir welding is larger than that of equilibrium by 3~5 orders of magnitude, and the atomic diffusion in this condition has the characters of super diffusion. In 1963, Balluffi et al. [118] indicated that the diffusion was promoted by severe deformation. Since then, this phenomenon has been found in a series of large deformation experiments, such as mechanical alloying [119], ultrasonic welding [120], and accumulative hot rolling [121, 122]. Sauvage et al. [121] investigated the distribution of Mg of aluminum alloys after severe plastic deformation and revealed that Mg atoms agglomerate on grain boundaries, forming mostly nanoscaled clusters at room temperature, as shown in Fig. 31. Both the contribution of dislocations and deformation-induced vacancies were considered to account for the enhanced mobility of Mg atoms. Xiong [123] and Qian [124] et al. also found the ultrafast atomic diffusion in friction stir processing of Al-Ni, Al-Ti alloys. Sauvage et al. [125] obtained Cu-Fe composite material by means of mechanical alloying and identified the formation of Cu-based supersaturated solid solution of 20 at.% Fe in the large deformation process, although mutual solubility of Cu and Fe at room temperature was very small in Cu-Fe

equilibrium conditions. They also found that the mutual diffusion was deeper where the grain was smaller, and the diffusion coefficient increased 19 orders of magnitude in comparison of which in equilibrium state, while the 4 orders of magnitude were composed by vacancies motivation. The experimental results showed that the atomic diffusion coefficient under large deformation was $10^3 \sim 10^8$ times than that of the thermal active diffusion, which was called super diffusion.

## 6 Summary and future outlook

Friction stir welding, as a solid-state welding method, has great advantages in joining various dissimilar aluminum alloys and steels with quite different physical or chemical properties, which could not be possible for a conventional welding technique. However, it still faces great challenges before it can be implemented extensively for dissimilar aluminum alloys and steels in wide ranging industries. The long service life of FSW tool with minimum wear is critical during Al/steel welding. The choice of tool materials and the design of tool shape are important for preventing IMC thickening, and forming either a metallurgical bonding or a mechanical interlocking via pin stirring and scribing. The coating technology that can reduce tool wear should also be studied. One of the critical challenges to bring Al/steel dissimilar joints to practical application is reliability and durability. To increase the material mixing between dissimilar aluminum alloys and steels and improve the joint mechanical performance, hybrid dissimilar welding by incorporating additional heat source, such as laser and arc, to soften the hard material was



**Fig. 31** Mg-rich zones in the AlMg alloy severely deformed at room temperature [121]. **a** STEM-HAADF image, **b** corresponding EDS map (Al–K blue, Sc–K green, and Mg–K red), **c** APT data and 3-D reconstruction showing nanoscaled Mg-rich clusters (Mg atoms are plotted in red and Al atoms in blue), and **d** 2-D Mg chemical map computed across these clusters showing that their Mg content is about10 at.% and locally up to 20 at.%
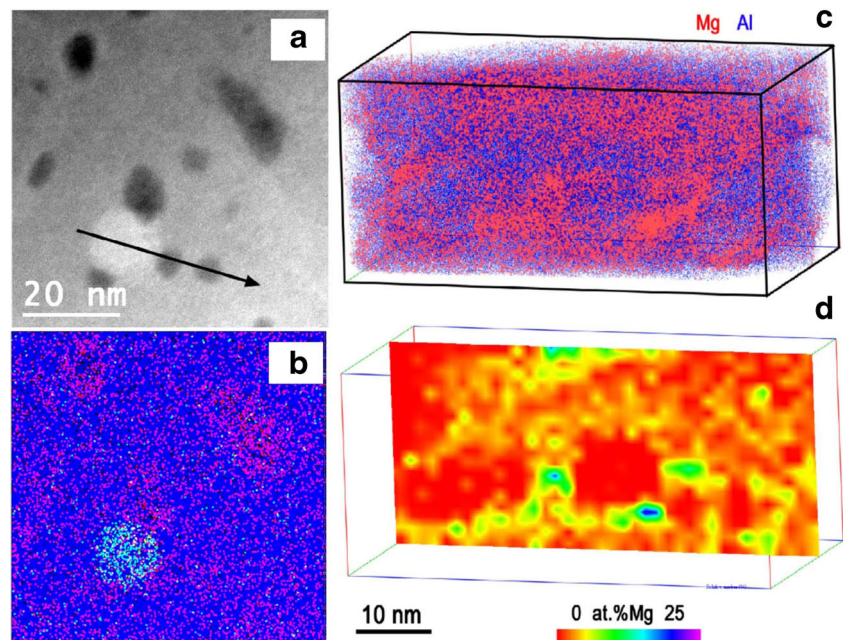
developed. The great mass of the existing literatures focuses on exploring the influence of welding conditions on weldability and their static performance, and very limited research has been given to repeatability of the welds and the fatigue performance. The fatigue performance of Al/steel joints needs to be fully explored. The formation of IMCs and other reactions has been seen in most of the dissimilar materials FSW with different base metals. The formation and growth of these IMCs are very rapid as a result of enhanced diffusion during welding. The thickness of IMC can be reduced in some cases by reducing the frictional heat input or using a third media to quickly take away the heat. The reduction in thickness of IMC can improve the weld strength significantly. On the other hand, formation of preferable IMC which is strong but less brittle through alloying or introducing an intermedia coating or transition layer can also contribute to strength improvement. Attention should be paid in the future to understand IMC formation and growth mechanisms, and explore alloying addition that can retard diffusion pathways or create less harmful IMC. With further research efforts and an increased understanding of the FSW process, an increasing number of applications will be found for FSW in the fabrication of Al/steel composite structure with high quality. Although a number of challenges still exist, FSW offers very attractive possibilities for commercial success.

**Publisher's Note** Springer Nature remains neutral with regard to jurisdictional claims in published maps and institutional affiliations.

# References

1. Kochan A (2002) A time of change for welding. Assembly Autom 22(1):29–35
2. Michalos G, Makris S, Papakostas N, Mourtzis D, Chryssolouris G (2010) Automotive assembly technologies review: challenges and outlook for a flexible and adaptive approach. CIRP J Manuf Sci Technol 2(2):81–91
3. Ermolaeva NS, Castro MBG, Kandachar PV (2004) Materials selection for an automotive structure by integrating structural optimization with environmental impact assessment. Mater Des 25(8):689–698
4. Coelho RS, Kostka A, dos Santos JF, Kaysser-Pyzalla A (2012) Friction-stir dissimilar welding of aluminum alloy to high strength steels: mechanical properties and their relation to microstructure. Mater Sci Eng A 556:175–183
5. Coelho RS, Kostka A, dos Santos JF, Pyzalla AR (2008) EBSD technique visualization of material flow in aluminum to steel friction-stir dissimilar welding. Adv Eng Mater 10(12):1127–1133
6. Tanaka T, Morishige T, Hirata T (2009) Comprehensive analysis of joint strength for dissimilar friction stir welds of mild steel to aluminum alloys. Scr Mater 61:756–759
7. Watanabe T, Takayama H, Yanagisawa A (2006) Joining of aluminum alloy to steel by friction stir welding. J Mater Process Tech 178:342–349
8. Chen CM, Kovacevic R (2005) Joining of Al 6061 alloy to AISI 1018 steel by combined effects of fusion and solid state welding. Int J Mach Tools Manuf 44:1205–1214
9. Uzun H, Donne CD, Argagnotto A, Ghidini T, Gambaro C (2005) Friction stir welding of dissimilar Al 6013-T4 to X5CrNi18-10 stainless steel. Mater Des 26:41–46
10. Won-Bae L, Martin S, Ulises AM, Gerhard B, Seung-Boo J (2006) Interfacial reaction in steel–aluminum joints made by friction stir welding. Scr Mater 55:355–358
11. Springer H, Kostka A, dos Santos JF, Raabe D (2011) Influence of intermetallic phases and Kirkendall-porosity on the mechanical properties of joints between steel and aluminum alloys. Mater Sci Eng A 528:4630–4642
12. Dilthey U, Stein L (2006) Multimaterial car body design: challenge for welding and joining. Sci Technol Weld Joi 11:135–142
13. Sajan SG, Meshram M, Pankaj S, Dey SR (2013) Friction stir welding of aluminum 6082 with mild steel and its joint analyses. Int J Adv Mater Manuf Charact 3:1–6
14. Ghosh M, Kar A, Kumar K, Kailas S (2012) Structural characterization of reaction zone for friction stir welded aluminum-stainless steel joint. Mater Technol Adv Perform Mater 27:169–172
15. Saida K, Song W, Nishimoto K (2005) Diode laser brazing of aluminum alloy to steels with aluminium filler metal. Sci Technol Weld Join 10(2):227–235
16. Dong HG, Liao CQ, Chen GQ, Dong C (2012) Butt joining of aluminum to steel by arc brazing process. Mater Manuf Process 27(12):1392–1396
17. Cai W, Wang P, Yang W (2005) Assembly dimensional prediction for selfpiercing riveted aluminum panels. Int J Mach Tools Manuf 45:695–704
18. Abe Y, Kato T, Mori K (2006) Joinability of aluminum alloy and mild steel sheets by self-piercing rivet. J Mater Process Technol 177:417–421
19. Yan WM, Xie ZQ, Yu C, Song LL, He HX (2017) Experimental investigation and design method for the shear strength of self-piercing rivet connections in thin-walled steel structures. J Construc Steel Res 133:231–240
20. Chen SH, Ma K, Huang JH, Xia J, Zhang H, Zhao XK (2011) Microstructure and mechanical property of joint by TIG welding brazing with dual weld pools for steel/aluminum dissimilar metals. Chin J Nonfer Metals 21(12):3076–3081
21. He H, Yang C, Lin S, Fan C, Chen Z, Chen Z (2014) Flux modification for AC-TIG braze welding of aluminum to stainless steel. Sci Technol Weld Join 19:527–533
22. Saida K, Ohnishi H, Nishimoto K (2010) Fluxless laser brazing of aluminum alloy to galvanized steel using a tandem beam-dissimilar laser brazing of aluminum alloy and steels. Weld Int 24(3):161–168
23. Jácome LA, Weber S, Leitner A, Arenholz E, Bruckner J, Hackl H, Pyzalla AR (2009) Influence of filler composition on the microstructure and mechanical properties of steel-aluminum joints produced by metal arc joining. Adv Eng Mater 11(5):350–358
24. Geiger M, Duflou J, Kals HJJ, Shirvani B, Singh UP (2005) Joining of steel-aluminum hybrid structures with electron beam on atmosphere. Adv Mater Res 6:143–150
25. Wang T, Zhang YY, Li XP, Zhang BG, Feng JC (2017) Influence of beam current on microstructures and mechanical properties of electron beam welding-brazed aluminum-steel joints with an Al5Si filler wire. Vacuum 141:281–287
26. Ye Z, Huang JH, Gao W, Zhang YF, Cheng Z, Chen SH, Yang J (2017) Microstructure and mechanical properties of 5052 aluminum alloy/mild steel butt joint achieved by MIG-TIG double-sided arc welding-brazing. Mater Des 123:69–79

27. Huang JK, He J, Yu XQ, Li CL, Fan D (2017) The study of mechanical strength for fusion-brazed butt joint between aluminum alloy and galvanized steel by arc-assisted laser welding. J Manuf Proces 25:126–133

28. Dong HG, Yang LQ, Dong C, Kou SD (2012) Improving arc joining of Al to steel and Al to stainless steel. Mater Sci Eng A 534:424–435

29. Shi Y, Zhang G, Huang Y, Lu L, Huang J, Shao Y (2014) Pulsed double electrode GMAW brazing for joining of aluminum to steel. Weld J 93:216–224

30. Movahedi M, Kokabi AH, Reihani SMS, Najafi H (2012) Effect of tool travel and rotation speeds on weld zone defects and joint strength of aluminum-steel lap joints made by friction stir welding. Sci Technol Weld Join 17:162–167

31. Thomas WM, Nicholas ED, Needham JC, Murch MG, Templesmith P, Dawes CJ (1991) G B Patent Application No. 9125978.8

32. Mishra RS, Ma ZY (2005) Friction stir welding and processing. Mater Sci Eng R 50:1–78

33. Nandan R, DebRoy T, Bhadeshia HKDH (2008) Recent advances in friction stir welding-process, weldment structure and properties. Prog Mater Sci 53:980–1023

34. Singh KV, Hamilton C, Dymek S (2010) Developing predictive tools for friction stir weld quality assessment. Sci Tech Weld Join 15:142–148

35. Teimournezhad J, Masoumi A (2010) Experimental investigation of onion ring structure formation in friction stir butt welds of copper plates produced by non-threaded tool pin. Sci Tech Weld Join 15:166–170

36. Moraitis GA, Labeas GN (2010) Investigation of friction stir welding process with emphasis on calculation of heat generated due to material stirring. Sci Tech Weld Join 15:177–184

37. Yadava MK, Mishra RS, Chen YL, Carlson B, Grant GJ (2010) Study of friction stir joining of thin aluminum sheets in lap joint configuration. Sci Tech Weld Join 15:70–75

38. Thomas WM, Threadgill PL, Nicholas ED (1999) Feasibility of friction stir welding steel. Sci Tech Weld Join 4(6):365–372

39. Bhadeshia H, DebRoy T (2009) Critical assessment: friction stir welding of steels. Sci Tech Weld Join 14(3):193–196

40. Cam G (2011) Friction stir welded structural materials: beyond Al-alloys. Int Mater Rev 56(1):1–48

41. Jiang WH, Kovacevic R (2004) Feasibility study of friction stir welding of 6061-T6 aluminum alloy with AISI1018 steel. Eng Manuf 218:1323–1331

42. Rafiei R, Moghaddam AO, Hatami MR, Khodabakhshi F, Abdolahzadeh A, Shokuhfar A (2017) Microstructural characteristics and mechanical properties of the dissimilar friction-stir butt welds between an Al–Mg alloy and A316L stainless steel. Int J Adv Manuf Technol 90:2785–2801

43. Chen T (2009) Process parameters study on FSW joint of dissimilar metals for aluminum-steel. J Mater Sci 44(10):2573–2580

44. Kimapong K, Watanabe T (2005) Effect of welding process parameters on mechanical property of FSW lap joint between aluminum alloy and steel. Mater Trans 46(10):2211–2217

45. Elrefaey A, Gouda M, Takahashi M, Ikeuchi K (2005) Characterization of aluminum/steel lap joint by friction stir welding. J Mater Eng Perform 14(1):10–17

46. Ogura T, Nishida T, Tanaka Y, Nishida H, Yoshikawa S, Fujimoto M (2013) Microscale evaluation of mechanical properties of friction stir welded A6061 aluminium alloy/304 stainless steel dissimilar lap joint. Sci Tech Weld Join 18:108–113

47. Elrefaey A, Takahashi M, Ikeuhi K (2005) Friction stir welded lap joint of aluminum to zinc-coated steel. Proc Jpn Weld Soc 23(2): 186–193

48. Merklein M, Giera A (2008) Laser assisted friction stir welding of drawable steel-aluminum tailored hybrids. Int J Mater Form 1: 1299–1302

49. Xing L, Ke LM, Huang CP (2007) Weld appearances and mechanical properties of friction stir welded joint of Al alloy and mild steel. Trans China Weld Instit 28(1):29–32

50. Habibnia M, Shakeri M, Nourouzi S, Givi MKB (2015) Microstructural and mechanical properties of friction stir welded 5050 Al alloy and 304 stainless steel plates. Int J Adv Manuf Technol 76:819–829

51. Ghosh M, Gupta RK, Husain MM (2014) Friction stir welding of stainless steel to Al alloy: effect of thermal condition on weld nugget microstructure. Metal Mater Trans A 45:854–863

52. Liu X, Lan SH, Ni J (2014) Analysis of process parameters effects on friction stir welding of dissimilar aluminum alloy to advanced high strength steel. Mater Des 59:50–62

53. Fukumoto M, Tsubaki M, Yasui T, Shimoda Y (2005) Joining of ADC12 and SS400 by means of friction stir welding. Weld Intern 19:364–369

54. Shen Z, Chen Y, Haghshenas M, Gerlich AP (2015) Role of welding parameters on interfacial bonding in dissimilar steel/ aluminum friction stir welds. Eng Sci Technol Int J 18:270–277

55. Yasui T, Tsubaki M, Fukumoto M, Shimoda Y, Ishii T (2006) High-speed weldability between 6063 and S45C by friction stir welding. Weld Intern 20(4):284–289

56. Kundu S, Roy D, Bhola R, Bhattacharjee D, Mishra B, Chatterjee S (2013) Microstructure and tensile strength of friction stir welded joints between interstitial free steel and commercially pure aluminum. Mater Des 50:370–375

57. Fei XJ, Jin XZ, Peng NX, Ye Y, Wu SG, Dai HF (2016) Effects of filling material and laser power on the formation of intermetallic compounds during laser-assisted friction stir butt welding of steel and aluminum alloys. Appl Phys A Mater Sci Process 122:936

58. Leitao C, Arruti E, Aldanondo E, Rodrigues DM (2016) Aluminum-steel lap joining by multipass friction stir welding. Mater Des 106:153–160

59. Xiong JT, Li JL, Qian JW, Zhang FS, Huang WD (2012) High strength lap joint of aluminium and stainless steels fabricated by friction stir welding with cutting pin. Sci Technol Weld Join 17: 196–201

60. Chen ZW, Yazdanian S, Littlefair G (2013) Effects of tool positioning on joint interface microstructure and fracture strength of friction stir lap Al-to-steel welds. J Mater Sci 48:2624–2634

61. Haghshenas M, Abdel-Gwad A, Omran AM, Gökçe B, Sahraeinejad S, Gerlich AP (2014) Friction stir weld assisted diffusion bonding of 5754 aluminum alloy to coated high strength steels. Mater Des 55:442–449

62. Liyanage T, Kilbourne J, Gerlich AP, North TH (2009) Joint formation in dissimilar Al alloy/steel and mg alloy/steel friction stir spot welds. Sci Tech Weld Join 14:500–508

63. Bozzi S, Helbert-Etter AL, Baudin T, Criqui B, Kerbiguet JG (2010) Intermetallic compounds in Al 6016/IF-steel friction stir spot welds. Mater Sci Eng A 527:4505–4509

64. Pourali M, Abdollah-zadeh A, Saeid T, Kargar F (2017) Influence of welding parameters on intermetallic compounds formation in dissimilar steel/aluminum friction stir welds. J Alloys Comp 715: 1–8

65. Collier M, Steel R, Nelson T, Sorensen C, Packer S (2003) Grade development of polycrystalline cubic boron nitride for friction stir processing of ferrous alloys. Mater Sci Forum 426-432(4):3011–3016

66. Rai R, De A, Bhadeshia HKDH, DebRoy T (2011) Review: friction stir welding tools. Sci Tech Weld Join 16:325–342

67. Sawada YK, Nakamura M (2009) Lapped friction stir welding between ductile cast irons and stainless steels. J Jpn Weld Soc 27:176–182

68. Choi DH, Lee CY, Ahn BW, Yeon YM, Park SHC, Sato YS, Kokawa H, Jung SB (2010) Effect of fixed location variation in friction stir welding of steels with different carbon contents. Sci Tech Weld Join 15:299–304

69. Shamsujjoha M, Jasthi BK, West M, Widener C (2015) Friction stir lap welding of aluminum to steel using refractory metal pin tools. J Eng Mater Technol 137(2):1–8

70. Mahto RP, Bhoje R, Pal SK, Joshi HS, Das S (2016) A study on mechanical properties in friction stir lap welding of AA 6061-T6 and AISI304. Mater Sci Eng A 652:136–144

71. Tanaka T, Hirata T, Shinomiy N, Shirakawa N (2015) Analysis of material flow in the sheet forming of friction-stir welds on alloys of mild steel and aluminum. J Mater Proc Technol 226:115–124

72. Patterson EE, Hovanski Y, Field DP (2016) Microstructural characterization of friction stir welded aluminum-steel joints. Metal Mater Trans A 7:2815–2829

73. Wei YN, Li JL, Xiong JT, Huang F, Zhang FS, Raza SH (2015) Joining aluminum to titanium alloy by friction stir lap welding with cutting pin. Mater Charact 71:1–5

74. Wei Y, Li J, Xiong J, Huang F, Zhang F (2012) Microstructures and mechanical properties of magnesium alloy and stainless steel weld-joint made by friction stir lap welding. Mater Des 33:111–114

75. Sorger G, Wang H, Vilaça P, Santos TG (2017) FSW of aluminum AA5754 to steel DX54 with innovative overlap joint. Weld World 61:257–268

76. Sun YF, Fujii H, Takaki N, Okitsu Y (2013) Microstructure and mechanical properties of dissimilar Al alloy/steel joints prepared by a flat spot friction stir welding technique. Mater Des 47:350–357

77. Uematsu Y, Kakiuchi T, Tozaki Y, Kojin H (2012) Comparative study of fatigue behavior in dissimilar Al alloy/steel and Mg alloy/steel friction stir spot welds fabricated by scroll grooved tool without probe. Sci Tech Weld Join 17(5):348–356

78. Li WY, Li JF, Zhang ZH, Gao DL, Wang WB, Dong CL (2014) Improving mechanical properties of pinless friction stir spot welded joints by eliminating hook defect. Mater Des 62:247–254

79. Zhang GF, Su W, Zhang JX, Wei ZX (2011) Friction stir brazing: a novel process for fabricating Al/steel layered composite and for dissimilar joining of Al to steel. Metall Mater Trans A 42:2850–2861

80. Chen YC, Komazaki T, Kim YG, Tsumura T, Nakata K (2007) Int Weld Join Conf., Seoul, Korea, 435–436

81. Kimapong K, Watanabe T (2004) Friction stir welding of aluminum alloy to steel. Weld J 12:277–282

82. Yazdipour A, Heidarzadeh A (2016) Effect of friction stir welding on microstructure and mechanical properties of dissimilar Al 5083-H321 and 316L stainless steel alloy joints. J Alloys Comp 680:595–603

83. van der Rest C, Jacques PJ, Simar A (2014) On the joining of steel and aluminum by means of a new friction melt bonding process. Scr Mater 77:25–28

84. Evans W, Gibson B, Reynolds J, Strauss A, Cook G (2015) Friction stir extrusion: a new process for joining dissimilar materials. Manuf Lett 5:25–28

85. Huang YX, Wang JC, Wan L, Meng XC, Liu HB, Li H (2016) Self-riveting friction stir welding of aluminum alloy to steel. Mater Lett 185:181–184

86. Bang HS, Bang HS, Jeon GH, Oh IH, Ro CH (2012) Gas tungsten arc welding assisted hybrid friction stir welding of dissimilar materials Al6061-T6 aluminum alloy and STS304 stainless steel. Mater Des 37:48–55

87. Bang HS, Bang HS, Hong JH, Jeon GH, Kim GS, Kapla AFH (2016) Effect of tungsten-inert-gas preheating on mechanical and microstructural properties of friction stir welded dissimilar Al alloy and mild steel. Strength Mater 48:152–159

88. Liu X, Lan SH, Ni J (2015) Electrically assisted friction stir welding for joining Al 6061 to TRIP780 steel. J Mater Proc Technol 219:112–123

89. Dehghani M, Amadeh A, Mousavi SAAA (2013) Investigations on the effects of friction stir welding parameters on intermetallic and defect formation in joining aluminum alloy to mild steel. Mater Des 49:433–441

90. Derazkola HA, Aval HJ, Elyasi M (2015) Analysis of process parameters effects on dissimilar friction stir welding of AA1100 and A441 AISI steel. Sci Tech Weld Join 20(7):553–562

91. Chen Y, Komazaki T, Tsumura T, Nakata K (2008) Role of zinc coat in friction stir lap welding Al and zinc coated steel. Mater Sci Tech 24:33–39

92. Chen YC, Komazaki T, Kim YG, Tsumura T, Nakata K (2008) Interface microstructure study of friction stir lap joint of AC4C cast aluminum alloy and zinc-coated steel. Mater Chem Phys 111:375–380

93. Jiang WH, Kovacevic R (2004) Feasibility study of friction stir welding of 6061-T6 aluminium alloy with AISI1018 steel. Eng Manuf 218:1323–1331

94. Kittipong K, Takehiko W (2005) Lap joint of A5083 aluminum alloy and SS400 steel by friction stir welding. Mater Trans (4):835–841

95. Chen YC, Nakata K (2008) Effect of the surface state of steel on the microstructure and mechanical properties of dissimilar metal lap joints of aluminum and steel by friction stir welding. Metall Mater Trans A 39(8):1985–1992

96. Sato YS, Park SHC, Michiuchi M (2004) Constitutional liquation during dissimilar friction stir welding of Al and Mg alloys. Scr Mater 50(9):1233–1236

97. Movahedi M, Kokabi AH, Reihani SMS, Cheng WJ, Wang CJ (2013) Effect of annealing treatment on joint strength of aluminum/steel friction stir lap weld. Mater Des 44:487–492

98. Das H, Jana SS, Pal TK, De A (2014) Numerical and experimental investigation on friction stir lap welding of aluminum to steel. Sci Tech Weld Join 19:69–75

99. Danesh MH, Karimi TA (2003) Bond strength and formability of an aluminum–clad steel sheet. J Alloy Compd 361:138–143

100. Nishida T, Ogura T, Nishida H, Fujimoto M, Takahashi M, Hirose A (2014) Formation of interfacial microstructure in a friction stir welded lap joint between aluminum alloy and stainless steel. Sci Tech Weld Join 19:609–616

101. Ogura T, Saito Y, Nishida T, Nishida H, Yoshida T, Omichi N, Fujimoto M, Hirose A (2012) Partitioning evaluation of mechanical properties and the interfacial microstructure in a friction stir welded aluminum alloy/stainless steel lap joint. Scr Mater 66:531–534

102. Esmaeili A, Zareie RHR, Sharbati M, Besharati GMK, Shamanian M (2011) The role of rotation speed on intermetallic compounds formation and mechanical behavior of friction stir welded brass/aluminum 1050 couple. Intermetallics 19:1711–1719

103. Coelho RS, Kostka A, Sheikhi S, dos Santos JF, Pyzalla AR (2008) Microstructure and mechanical properties of an AA6181-T4 aluminum alloy to HC340LA high strength steel friction stir overlap weld. Adv Eng Mater 10:961–972

104. Das H, Ghosh RN, Pal TK (2014) Study on the formation and characterization of the intermetallics in friction stir welding of aluminum alloy to coated steel sheet lap joint. Metall Mater Trans A 45:5098–5106

105. Abbasi M, Dehghani M, Guim H, Kim D (2016) Investigation of Fe-rich fragments in aluminum-steel friction stir welds via simultaneous transmission Kikuchi diffraction and EDS. Acta Mater 117:262–269

106. Fei X, Jin X, Ye Y, Xiu T, Yang H (2016) Effect of pre-hole offset on the property of the joint during laser-assisted friction stir welding of dissimilar metals steel and aluminum alloys. Mater Sci Eng A 653:43–52

107. Potesser M, Schoeberl T, Antrekowitsch H, Bruckner J (2006) The characterization of the intermetallic Fe-Al layer of steel-aluminum weldings. In: EPD Congress 2006. Curran Associates Incorporated, New York, pp 167–176

108. Schmidt H, Hattel J, Wert J (2004) An analytical model for the heat generation in friction stir welding. Model Simul Mater Sci Eng 12(1):143–157

109. Ramachandran KK, Murugan N, Kumar SS (2015) Influence of tool traverse speed on the characteristics of dissimilar friction stir welded aluminium alloy, AA5052 and HSLA steel joints. Archives Civ Mech Eng 15(4):822–830

110. Ma ZY, Pilchak AL, Juhas MC, Williams JC (2008) Microstructural refinement and property enhancement of cast light alloys via friction stir processing. Scr Mater 58:361–366

111. Watanabe M, Feng KY, Nakamura Y, Kumai S (2011) Growth manner of intermetallic compound layer produced at welding interface of friction stir spot welded aluminum/steel lap joint. Mater Trans 52(5):953–959

112. Wang ZB, Lu J, Lu K (2005) Chromizing behaviors of a low carbon steel processed by means of surface mechanical attrition treatment. Acta Mater 53(7):2081–2089

113. Fukumoto S, Tsubakino H, Okita K, Aritoshi M, Tomita T (2000) Amorphization by friction welding between 5052 aluminum alloy and 304 stainless steel. Scr Mater 42(8):807–812

114. Su JY, Fujii H, Koji I, Sun YF, Yoshihiko Y, Hisamichi K, Akihisa I (2011) Fabrication of Fe based metallic glass particle reinforced Al-based composite materials by friction stir processing. Mater Trans 52:1634–1640

115. Tarasov SY, Rubtsov VE, Kolubaev EA (2014) A proposed diffusion-controlled wear mechanism of alloy steel friction stir

welding (FSW) tools used on an aluminum alloy. Wear 318: 130–134

116. ben-Avraham D, Havlin S (2000) Diffusion and reactions in fractals and disordered systems. Cambridge University Press

117. Havlin S, ben-Avraham D (2002) Diffusion in disordered media. Adv Phys 51:187–292

118. Balluffi RW, Ruoff AL (1963) On strain-enhanced diffusion in metals: I. Point defect models. J Appl Phys 34(6):1634–1647

119. Das D, Chatterjee PP, Manna I, Pabi S (1999) Measure of enhanced diffusion kinetics in mechanical alloying of Cu–18 at.% Al by planetary ball milling. Scr Mater 41(8):861–866

120. Li MY, Ji HJ, Wang CQ, Han SB, Bang HS (2006) Interdiffusion of Al–Ni system enhanced by ultrasonic vibration at ambient temperature. Ultrasonics 45(1–4):61–65

121. Sauvage X, Enikeev N, Valiev R, Nasedkina Y, Murashkin M (2014) Atomic-scale analysis of the segregation and precipitation mechanisms in a severely deformed Al–Mg alloy. Acta Mater 72(15):125–136

122. Sauvage X, Jessner P, Vurpillot F, Pippan R (2008) Nanostructure and properties of a Cu–Cr composite processed by severe plastic deformation. Scr Mater 58(12):1125–1128

123. Xiong JT, Zhang FS, Li JL, Qian JW, Huang WD (2010) In-situ synthesized Al3Ni-Al composites by friction stir processing. Rare Metal Mater Eng 39(1):139–143

124. Qian JW, Li JL, Xiong JT, Zhang FS, Lin X (2010) In-situ synthesized Al3Ti-Al surface composites by friction stir processing. Trans China Weld Ins 31(8):61–64

125. Sauvage X, Wetscher F, Pareige P (2005) Mechanical alloying of cu and Fe induced by severeplastic deformation of a Cu–Fe composite. Acta Mater 53(7):2127–2135